



doi:10.1016/S0016-7037(00)01344-3

## Climatic significance of seasonal trace element and stable isotope variations in a modern freshwater tufa

CHRISTIAN IHLENFELD,<sup>1,\*</sup> MARC D. NORMAN,<sup>2</sup> MICHAEL K. GAGAN,<sup>3</sup> RUSSELL N. DRYSDALE,<sup>4</sup> ROLAND MAAS,<sup>1</sup> and JOHN WEBB<sup>1</sup><sup>1</sup>Department of Earth Sciences, La Trobe University Melbourne, Bundoora, Vic. 3086, Australia<sup>2</sup>Centre of Ore Deposit Research, The University of Tasmania, GPO Box 252-79, Hobart, Tas. 7001, Australia<sup>3</sup>Research School of Earth Sciences, The Australian National University, Canberra, ACT 0200, Australia<sup>4</sup>School of Geosciences, The University of Newcastle, Callaghan, NSW 2308, Australia

(Received July 23, 2001; accepted in revised form October 1, 2002)

**Abstract**—We present a continuous ~14-yr-long (1985 to 1999) high-resolution record of trace element (Mg, Sr, Ba, U) and stable isotope ( $\delta^{13}\text{C}$ ,  $\delta^{18}\text{O}$ ) variations in a modern freshwater tufa from northwestern Queensland, Australia. By utilizing the temperature dependence of the  $\delta^{18}\text{O}$  signal, an accurate chronology was developed for the sampled profile, which allowed a comparison of the chemical records with hydrological and meteorological observations. As a consequence, it was possible to constrain the relevant geochemical processes relating climate variables, such as temperature and precipitation, to their chemical proxies in the tufa record. Temperatures calculated from the Mg concentrations of the tufa samples provide close approximations of average annual water temperature variations. Furthermore, we demonstrate that temporal changes in  $(\text{Mg}/\text{Ca})_{\text{water}}$  can be estimated using an empirically derived equation relating  $(\text{Mg}/\text{Ca})_{\text{water}}$  to the  $(\text{Sr}/\text{Ba})$  ratio measured in the tufa samples. By means of this relationship, it is theoretically possible to determine the  $(\text{Mg}/\text{Ca})$  ratio of paleowaters, and hence to derive reliable estimates of former water temperatures from the Mg concentrations of fossil tufas from the study area. Sympathetic variations in Sr, Ba, and  $\delta^{13}\text{C}$  along the sampled profile record changes in water chemistry, which are most probably caused by variable amounts of calcite precipitation within the vadose zone of the karst aquifer. This process is thought to be markedly subdued whenever the amount of wet-season precipitation exceeds a given threshold. Accordingly, distinct minima in Sr, Ba, and  $\delta^{13}\text{C}$  are interpreted to reflect years with above-average rainfall. The pronounced seasonal and annual variability of the U concentration along the profile is thought to primarily record changes in the U flux from the soil to the water table. We suggest that during intensive rain events U is transported to the phreatic zone by complexing organic colloids, giving rise to conspicuous U maxima in the tufa after above-average wet seasons. This study demonstrates the potential of freshwater tufas to provide valuable information on seasonal temperature and rainfall variations. If tufa deposits turn out to be reasonably resistant to secondary processes, combined investigation of speleothems and tufas from the same area could become a promising approach in future research. While speleothems offer continuous records of long-term paleoenvironmental changes, tufas could provide high-resolution time windows into selected periods of the past. Copyright © 2003 Elsevier Science Ltd

### 1. INTRODUCTION

Paleoclimate research has made appreciable progress in elucidating the response of important climate phenomena, such as the intertropical monsoons and the El Niño–Southern Oscillation, to internal (i.e., interaction among the atmosphere, oceans, land surface and ice sheets) and external forcing (i.e., orbitally driven changes in solar radiation). To further improve our understanding of the complex dynamics of these climate processes, it is necessary to quantify how long-term fluctuations affect their high-frequency variability. Coral records in particular have proven to be capable of addressing this question (e.g., Charles et al., 1997; Tudhope et al., 2001). To complement data retrieved from these marine archives, high-resolution terrestrial records are needed. Furthermore, quantitative or semiquantitative seasonal paleoclimate information for continental interiors is essential to verify climate model predictions (e.g., Montoya et al., 1998).

Among the various terrestrial records, speleothems have

been of particular interest in studies of Quaternary climate change in recent years (e.g., Bar-Matthews et al., 1997, 1999; Ayalon et al., 1999; McDermott et al., 1999; Hellstrom and McCulloch, 2000). Speleothems form across a wide range of climatic zones, provide long, continuous, and commonly well preserved records, and can be accurately dated over the last several hundred thousand years. Paleoenvironmental changes are potentially recorded in speleothems by a number of physical and chemical proxies, including variations in their trace element and stable isotope composition. However, due to their low growth rates on the order of  $10^0$  to  $10^2 \mu\text{m yr}^{-1}$  (e.g., Baker et al., 1998), the temporal resolution achievable by conventional, i.e., mechanical, microsampling is usually limited to  $>10^1$  yr. Applying more sophisticated analytical techniques, such as secondary ionization mass spectrometry or laser-ablation inductively coupled plasma mass spectrometry, it is potentially possible to reveal annual trace element cycles in speleothems (Roberts et al., 1998, 1999; Huang et al., 2001). The interpretation of such data, however, is hampered by the increasing importance of crystal surface structure and growth mechanisms for the trace element partitioning, as the size of analytical spots approaches the size of individual crystals (e.g.,

\* Author to whom correspondence should be addressed (C.Ihlenfeld@latrobe.edu.au).

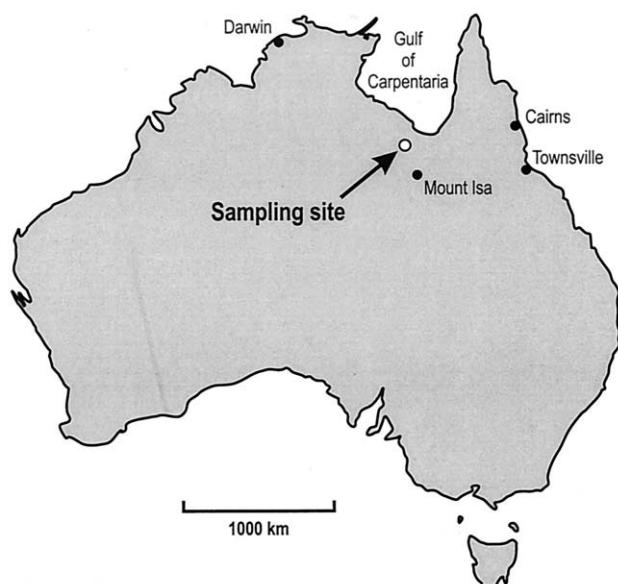


Fig. 1. Location map for the sampling site.

Paquette and Reeder, 1995; Huang and Fairchild, 2001). In addition, the importance of site-specific effects for individual speleothem trace element and stable isotope records sets limits to their general reliability as archives of paleoenvironmental information (Bar-Matthews et al., 1996; Roberts et al., 1999).

Despite the limitations of speleothems, other terrestrial records potentially offering high temporal resolution, such as freshwater tufas, have surprisingly received little attention. Several studies on freshwater tufas have demonstrated that valuable environmental information can be preserved in these deposits (e.g., Pazdur et al., 1988; Andrews et al., 1993, 1994, 1997, 2000). These previous studies, however, utilized exclusively stable isotope systematics as indicators of environmental conditions, and neglected the potential of trace elements in paleoclimate reconstruction, as well as the possibility of systematic subseasonal sampling.

The purpose of this article is to investigate whether fluvial tufas can provide useful annual and intra-annual climate information suitable for high-resolution paleoclimate reconstruction. We present a continuous ~14-yr-long (1985 to 1999) trace element (Mg, Sr, Ba, U) and stable isotope ( $\delta^{13}\text{C}$ ,  $\delta^{18}\text{O}$ ) record from a modern tufa, and discuss the relevant geochemical processes governing the observed variations in these parameters. Development of a reliable time series for the sampled profile allows us to compare the chemical records with hydrological and meteorological observations, in order to define their climatic significance.

### 1.1. General Setting

The tufa sample for this study was collected in July 1999 from a site along the Gregory River in northwestern Queensland, Australia. The location lies ~200 km south of the Gulf of Carpentaria, in vicinity to the Riversleigh homestead (Fig. 1). The area is characterized by a semiarid monsoon climate, with ~90% of the annual rainfall occurring during the wet season

from November to March. Discharge of the Gregory River is perennial but varies seasonally in response to the monsoonal rainfall distribution. The river drains a karst catchment located to the west and southwest of the sampling site. The size of the catchment upstream of the sampling location is ~5500 km<sup>2</sup>. Its elevation ranges from 140 m to 260 m above sea level. The lithology of the karst plateau consists of Middle Cambrian limestones close to the eastern edge of the catchment, and Upper Proterozoic or Lower Cambrian dolomites further upstream. The plateau is covered by a black residual clay soil of variable and westward increasing thickness of 0 to >0.5 m. The vegetation in the catchment is characteristic of a dry savanna and comprises both C<sub>3</sub> (shrubs, scattered trees) and C<sub>4</sub> (grasses) plants (e.g., Johnson et al., 1999).

Apart from a few very minor deposits within the karst terrain, major tufa deposition commences ~2 km downstream of the escarpment, where the river enters a Lower Proterozoic siltstone, sandstone, and greywacke lithology. The sample analyzed in this study (Fig. 2) was deposited at the base on the downstream side of a tufa barrage, ~4.5 km from the escarpment. Water flow rates at this site are moderately fast, making both microenvironmental effects (e.g., Andrews et al., 1997) and erosive episodes unlikely. Periodical drying out of the site during dry spells is not probable because the water level is buffered by the tufa barrages, which dam up the water behind their structures.

### 1.2. Temperature and Precipitation Records

The hydrological and meteorological information, which is necessary for an interpretation of the trace element and isotope records in terms of their climatic significance, were obtained from the Department of Natural Resources Queensland and the Australian Bureau of Meteorology, respectively. River discharge and water temperature are recorded at a gauging station ~8 km downstream of the sampling location. A complete series of total monthly discharge data is available, except for the time from October 1988 to May 1991, when the station was closed. Water temperature has been continuously measured at the station since December 1996. Before that time, only three to four sporadic temperature measurements were performed every year. Complete records of monthly average air temperature and total monthly precipitation are available for six weather stations surrounding the sampling location (Wollogorang, Burketown, Normanton, Brunette Downs, Mount Isa, Cloncurry). None of these stations is in close proximity to the sampling site, however. Therefore, the best estimation of air temperature and precipitation in the study area is thought to be a weighted average of the six records, with weighting factors being the reciprocals of the distance from the weather station to the sampling location (temperature), or the center of the catchment (precipitation), respectively. This approach appears to be reasonable because topography, which potentially could influence temperature and precipitation at an individual site, is uniformly low in the entire region.

Comparison of the composite air temperature record with the water temperatures measured at the gauging station shows that the two oscillations are strongly synchronous. The water temperatures, however, are systematically offset to higher values. The offset is different for individual months of a single year,

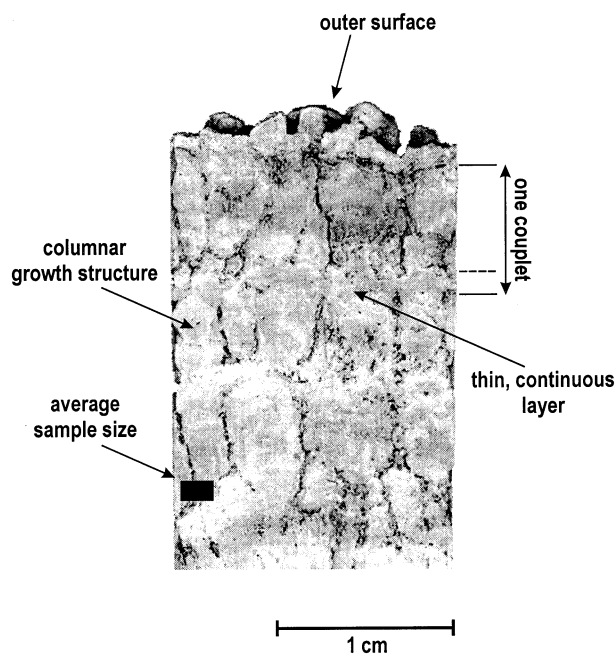


Fig. 2. Enlarged section of the sampled tufa slab. The outer surface corresponds to mid-July 1999, when the sample was collected. Visible is the alternation of thin, continuous layers and relatively thick layers consisting of columnar structures. According to Chafetz et al. (1991), a couplet comprising a thin and a thick layer is assumed to represent one annual cycle. The black rectangle indicates the average size of individual samples. See sections 2.1 and 4.1.1 for discussion.

but more or less constant for the same month of different years. The lowest offset is observed during the wet season ( $\sim 0.8^{\circ}\text{C}$ ), the highest during the dry season ( $\sim 1.4^{\circ}\text{C}$ ). The best explanation for this seasonally varying positive temperature offset is solar heating of the river water, which is reduced during the wet season by increased cloud cover. In order to extend the water temperature record further back in time, we modeled the water temperature by adding the average offset during the respective month to the average monthly air temperatures of the composite record. The water temperatures calculated this way are in fairly good agreement with the actual values of the continuous water temperature record (since December 1996) and the sporadic temperature measurements (before December 1996). The average deviation between modeled and observed values is  $0.0 \pm 0.5^{\circ}\text{C}$  ( $1\sigma$ ).

## 2. MATERIALS AND METHODS

### 2.1. Tufa Sample

The tufa sample from Gregory River was subjected to careful macroscopic, microscopic and mineralogical examination. Calcite, the only phase detectable by X-ray diffraction analysis of bulk powders, is the major constituent of the tufa. Inorganic impurities insoluble in dilute acetic acid are minor and account for  $\sim 0.8$  wt%. X-ray diffraction and X-ray fluorescence spectrometry analyses of these impurities allowed to quantify the contents of individual phases: quartz ( $\sim 0.25$  wt%), kaolinite ( $\sim 0.35$  wt%), and nontronite-rich smectite ( $\sim 0.20$  wt%). The approximate concentrations of Mg and Ca in the insoluble residue are 0.8 wt% and 1.2 wt%, respectively. The amounts of Sr, Ba, and U were below detection limit. Organic material, readily perceptible by its green color, occurs in distinct horizons finely disseminated in the calcitic matrix. While no indications of erosive episodes (e.g., presence of

lithoclasts, erosion surfaces) or intermittent drying out of the sample site (e.g., growth hiatuses) could be found, microscopic investigation revealed the presence of minor calcitic cements, lining voids and pores. The microsparitic fabric of these secondary precipitates is readily distinguished from the micritic calcite of the tufa laminae. Evaluation of thin sections showed that cements account for  $\sim 0.5\%$  of the sample. No significant variation in the abundance of cements was observed in different portions of the tufa.

After the initial examination, a slab was cut from the tufa sample parallel to the axis of maximum growth, ultrasonically cleaned in a succession of Millipore water, double-distilled acetone, and Millipore water for 1 h each, and then air dried in a clean air hood. Repeated examination of the slab showed that the majority of the calcitic cements and most of the organic material were removed during the cleaning procedure. Eighty-three samples were then abraded in a continuous, 93.75-mm-long strip along an edge of the sample slab. During abrasion special care was taken not to mix material from distinct layers in individual samples. In order to minimize time-averaging of the chemical signals due to the slightly curved, uneven growth surfaces of the tufa, we abraded as small a surface area as was practical. The dimensions of individual samples are fairly constant along the profile, averaging 1.1 mm in thickness and  $1.6 \text{ mm} \times 1.6 \text{ mm}$  in cross section. To check for lateral reproducibility of the chemical records, a  $\sim 1$ -cm-long section between two marker horizons was sampled from another slab. Each sample was then ground and homogenized in an agate mortar, and subsequently split into aliquots for trace element and stable isotope analysis.

For trace element analysis, 1.5 to 3 mg of each sample was weighed in a Teflon beaker, immersed in Millipore water, and slowly dissolved by stepwise addition of 0.5 N nitric acid. To promote the oxidation of any remaining organic matter, a small amount of concentrated hydrogen peroxide was added to each sample. After complete dissolution the samples were further diluted to a factor of  $\sim 3000$  and analyzed on a HP4500 inductively coupled plasma mass spectrometer (ICP-MS) at the University of Tasmania. Variations in instrument sensitivity were corrected for by external standardization. Finally, all element concentrations were normalized to Ca in order to eliminate weighing errors which could be greater than 10% given the small sample sizes. Analytical precision of Ca-normalized concentrations is  $\sim 1\%$  (Relative standard deviation, RSD) for Sr and  $\sim 4\%$  (RSD) for Mg, Ba, and U, as assessed via the reproducibility of multiple analyses of a bulk tufa sample.

The sample aliquots for stable isotope analysis were not further pretreated prior to mass spectrometric measurement as it has been shown that cleaning protocols, such as vacuum roasting and hydrogen peroxide cleaning, do not improve sample reproducibility (McConaughey, 1989). Stable isotope measurements were carried out at the Australian National University (ANU; samples GMT-1 to GMT-36) and at Monash University (samples GMT-37 to GMT-83). At ANU, isotopic analyses were obtained by reacting  $\sim 0.20$  mg of each sample with 105% phosphoric acid at  $90^{\circ}\text{C}$  for 13 min in an automated individual-carbonate reaction (Kiel) device coupled with a Finnigan MAT-251 mass spectrometer. Isotope ratios are calibrated with the NBS-19 and NBS-18 carbonate standards. Reproducibility ( $2\sigma$ ) is  $\sim 0.05\%$  for  $\delta^{18}\text{O}$  and  $\sim 0.03\%$  for  $\delta^{13}\text{C}$ . At Monash University,  $\text{CO}_2$  was extracted from 2 to 3 mg of each sample by reaction with 105% phosphoric acid at  $25^{\circ}\text{C}$  for 12 to 18 h (McCrea, 1950), and subsequently measured on a fully automated Finnigan MAT-252 mass spectrometer. Standardization is against an in-house calcite standard which was calibrated with IAEA-CO-1. Long-term average  $\delta^{18}\text{O}$  and  $\delta^{13}\text{C}$  values of the in-house standard are  $12.68 \pm 0.13\%$  (Vienna standard mean ocean water; V-SMOW) and  $-6.37 \pm 0.06\%$  (Vienna Pee Dee Belemnite; V-PDB), respectively. Reproducibility ( $2\sigma$ ) is 0.1‰ for both  $\delta^{18}\text{O}$  and  $\delta^{13}\text{C}$ .

Repeat analyses of the in-house standard and several samples measured at Monash University were carried out at ANU to check the consistency of the two data sets. Comparison of the results revealed a very consistent, systematic deviation of the Monash data for both  $\delta^{18}\text{O}$  and  $\delta^{13}\text{C}$ . Therefore,  $\delta^{18}\text{O}$  and  $\delta^{13}\text{C}$  values of all samples measured at Monash University were corrected using empirically derived equations, resulting in a very good agreement between the two data sets. Deviation of the corrected Monash data from the respective ANU values is 0.00

$\pm 0.05\%$  ( $2\sigma$ ) for  $\delta^{18}\text{O}$  and  $0.00 \pm 0.04\%$  ( $2\sigma$ ) for  $\delta^{13}\text{C}$ , and thus less than the analytical reproducibility of 0.1%.

Throughout this article, O and C isotope ratios are reported as per mil (‰) deviations relative to V-SMOW and V-PDB, respectively.

## 2.2. Water and Bedrock Samples

Along with the tufa, we collected river water samples at the sampling site. Within hours of collection, all samples were passed through 0.45- $\mu\text{m}$  acetate cellulose filters, and bicarbonate alkalinity was determined by potentiometric titration using a Hach alkalinity titration kit. Samples for cation analysis were acidified with nitric acid, while unacidified samples were retained for anion and  $\delta^{18}\text{O}$  analysis. Electrical conductivity and pH of the river water were measured in situ at the sampling site.

Cation concentrations were determined at ANU on an Agilent Technologies HP7500 ICP-MS using external standardization to correct for variations in instrument sensitivity. The relative difference between replicate analyses is  $< 2\%$  for Mg, Ca, and U, and  $< 5\%$  for Sr and Ba. Oxygen isotope measurements were carried out at ANU on a Finnigan MAT-251 mass spectrometer after equilibration of 2 mL of water with  $\text{CO}_2$  for  $>30$  h at  $25^\circ\text{C}$  (Epstein and Mayeda, 1953). Isotope ratios, reported as per mil (‰) deviation relative to the V-SMOW standard, are calibrated with two in-house water standards. Reproducibility is  $\sim 0.04\%$  ( $2\sigma$ ).

To complement the available major and trace element data for bedrocks from the study area (Budd et al., 2000), we collected two dolomite samples. Aliquots of the powdered whole rock samples were analyzed at ANU on an Agilent Technologies HP7500 ICP-MS following a protocol very similar to the one previously described for the tufa samples. RSD of multiple analyses of a standard solution is  $\sim 2\%$  for Mg and Sr,  $\sim 3\%$  for U and  $\sim 4\%$  for Ca and Ba.

## 3. RESULTS

The trace element and stable isotope results are listed in Table A1 in the Appendix. Figure 3 shows the data plotted against the distance of the respective sample from the tufa surface. The tufa surface corresponds to July 1999, when the sample was collected. All correlation coefficients reported throughout this article are statistically significant at the 1% level.

The highly significant correlations existing between Sr and Ba ( $r = 0.80$ ), and to a slightly lesser degree between Sr and  $\delta^{13}\text{C}$  ( $r = 0.68$ ), imply that much of the variation observed in these three variables is controlled by either the same, or different but indirectly linked processes. In addition to their general synchronism, which is most pronounced for Sr and Ba, the patterns share distinctive features. The three records exhibit, for instance, similar variations in amplitude along the profile with larger amplitudes occurring in the middle section and smaller amplitudes toward the ends. Distinctive minima, generally more pronounced and conspicuous than maxima, are also common. Except for the  $\delta^{13}\text{C}$  minimum around 4.5 cm, these negative excursions are synchronous in all three records. Remarkable in this respect is the coincidence of the absolute minima in the same sample. While Sr exhibits no obvious trend over the entire profile, Ba and  $\delta^{13}\text{C}$  show opposite long-term trends, explaining the somewhat weaker relationship between these two variables ( $r = 0.40$ ).

U correlates significantly with Sr ( $r = 0.53$ ) and  $\delta^{13}\text{C}$  ( $r = 0.44$ ), which is apparent in their general synchronism and in the concurrence of their absolute minima. Both U and  $\delta^{13}\text{C}$  show a weak decreasing trend with time. However, despite these mutual features pointing to some common forcing factor, the U record differs from the patterns of Sr, Ba, and  $\delta^{13}\text{C}$  in its

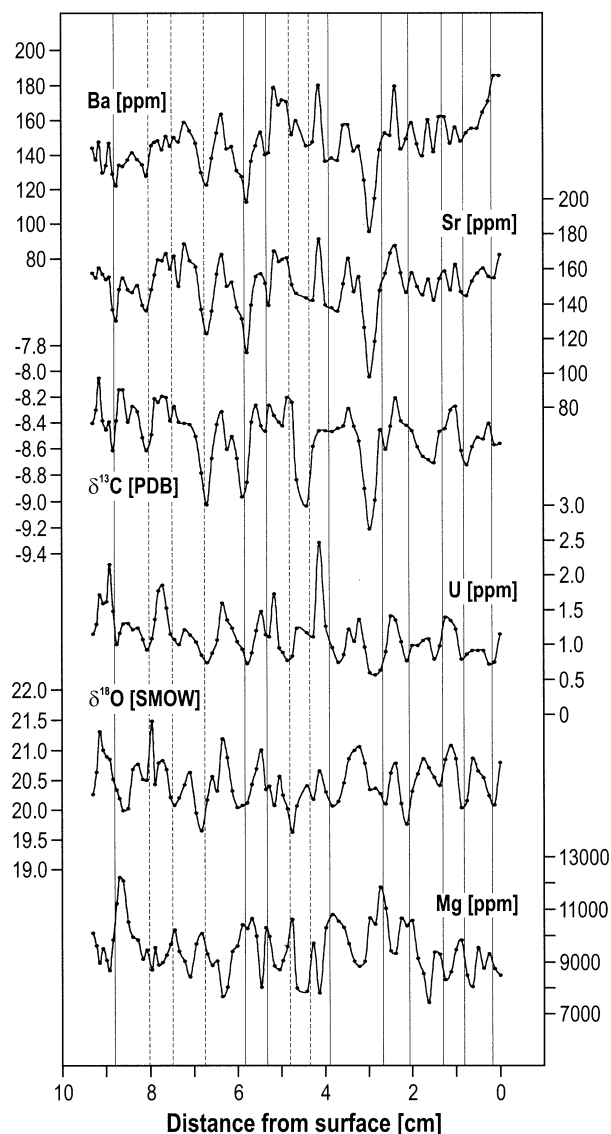


Fig. 3. Trace element and stable isotope results for the sampled tufa profile. Data are plotted vs. distance from the outer surface. Vertical lines mark the limits of consecutive couplets comprising a thin and a thick layer (see Fig. 2). The lines are solid where a thin, continuous layer is clearly developed, and dashed where it is less defined. The varve-like layering potentially provides useful annual time markers. Clearly perceptible is the variable thickness of the layers. Analytical precision is 1% (RSD) for Sr, 4% (RSD) for Mg, Ba, and U, and  $\leq 0.1\%$  for  $\delta^{13}\text{C}$  and  $\delta^{18}\text{O}$ . See sections 3 and 4.1 for discussion.

significantly larger relative amplitude, its conspicuous maxima, and a remarkable alternation of large and small local maxima. U is also related to the  $\delta^{18}\text{O}$  signal ( $r = 0.48$ ).

Contrasting with the patterns described above, the variation in  $\delta^{18}\text{O}$  is more regular along the profile. Deviations from this regular trend, such as the slight depression in the middle section of the record, are in general relatively small and inconspicuous. While  $\delta^{18}\text{O}$  is unrelated to Sr, Ba, and  $\delta^{13}\text{C}$ , it shows a significant anticorrelation with Mg ( $r = -0.54$ ), evident in the anticyclical variation of these two variables. However, in contrast to the relative regularity of the  $\delta^{18}\text{O}$  record, the Mg

Table 1. Hydrochemical data for the Gregory River at the tufa sampling site, mid-July 1999.

T (°C) <sup>a</sup>	21.9		
pH <sup>a</sup>	7.93		
SC (μS/cm) <sup>a</sup>	713		
log pCO <sub>2</sub> (atm) <sup>b</sup>	-2.35		
SI <sub>calcite</sub> <sup>b</sup>	0.92		
		Molar ratios	
HCO <sub>3</sub> (mg/L)	436	HCO <sub>3</sub> /Ca	3.374
Mg (mg/L)	53.0	Mg/Ca	1.028
Ca (mg/L)	85.0	—	—
Sr (μg/L)	120	Sr/Ca	6.4 × 10 <sup>-4</sup>
Ba (μg/L)	103	Ba/Ca	3.5 × 10 <sup>-4</sup>
U (μg/L)	1.2	U/Ca	2.4 × 10 <sup>-6</sup>
δ <sup>18</sup> O (‰ SMOW)	-7.87		

<sup>a</sup> Temperature, pH, and electrical conductivity were measured in situ at the sampling site.

<sup>b</sup> log pCO<sub>2</sub> and calcite saturation index (SI<sub>calcite</sub>) were calculated using the PCWATEQ computer program (Rollins, 1987).

concentration displays pronounced positive deviations at ~9 cm and around ~3 cm. The anticorrelations existing between Mg and Ba ( $r = -0.46$ ), U ( $r = -0.39$ ), Sr ( $r = -0.33$ ) suggest some direct or indirect link between their variations.

#### 4. DISCUSSION

Interpretation of this data set is constrained by our understanding of the mechanisms of tufa calcification. An issue of particular significance is the relative importance of biological and physicochemical controls on calcite precipitation. In CO<sub>2</sub>-rich streams, such as the Gregory River (Drysdale et al., 2002), where waters become highly supersaturated with respect to calcite as a result of CO<sub>2</sub> outgassing, active biological control on tufa calcification appears to be negligible (e.g., Pentecost and Riding, 1986; Merz-Preiss and Riding, 1999). Microbial mats and biofilms are thought to merely localize calcite precipitation in such environments by providing favorable nucleation sites (e.g., Merz-Preiss and Riding, 1999). The trace element and stable isotope geochemistry of the tufa is therefore likely to be controlled by physicochemical factors. Comparison between analyses of the outermost tufa sample (sample GMT-1; Table A1) and the water sample collected in July 1999 (Table 1) supports this interpretation. Trace element partitioning and oxygen isotope fractionation between these two samples are in quantitative agreement with published data from inorganic precipitation experiments, as will be shown in the following sections. We assume, therefore, that the tufa was precipitated in approximate isotopic equilibrium with the ambient water and dissolved inorganic carbon, which has been demonstrated in previous studies on tufas from riverine settings similar to the one described here (e.g., Chafetz et al., 1991; Andrews et al., 1997). Various effects may have disrupted the isotopic equilibrium slightly, but since our data set can be logically interpreted on the basis of equilibrium principles, we doubt that these effects seriously detract from our interpretations. Similar assumptions can be made regarding the trace element incorporation into the tufa. In this case, however, the term “equilibrium” refers to a quantitative agreement with appropriate partitioning coefficients rather than to a real thermodynamic equilibrium. Any crystallographic control on trace

element partitioning and stable isotope fractionation (e.g., Dickson, 1991; Paquette and Reeder, 1995) can be ignored in the discussion of the present data set because the size of individual samples is much greater than the size of single crystallites.

The potential impact of inorganic impurities (section 2.1) on the trace element records may be assessed by using the Th concentrations given in Table A1. Since Th is virtually insoluble in water under the pH conditions of the Gregory River (Langmuir and Herman, 1980; Table 1), the bulk of Th in the tufa must be associated with non-carbonate phases. The strong relationships between Th and transition metals such as Sc ( $r = 0.87$ ) and Ti ( $r = 0.80$ ) support this interpretation (data not presented). Given that the dissolution procedure was identical for all samples, their Th concentrations may be used as a proxy for the variable amount of such impurities along the profile. Thus, the lack of correlation between Th and Mg-Sr-Ba-U suggests that contributions of these elements from noncarbonate impurities are insignificant. It is therefore valid to presume that all trace element variations considered here reflect compositional changes of the tufa calcite.

Any significant influence of calcitic pore fillings on the results can also be ruled out on the basis of the careful examination of the sample outlined earlier (section 2.1). The continuity of the tufa record is evident from the absence of obvious growth hiatuses or erosion surfaces. Its lateral reproducibility was confirmed in this study by the analyses of a ~1-cm-long section from another slab (data not shown).

#### 4.1. Time-Series Development

##### 4.1.1. Stratigraphic Time Markers

In order to compare the data sets with available meteorological and hydrological data, it is essential to develop a reliable and sufficiently precise time series for the tufa record. Approximate time markers are potentially provided by the lamination of the tufa because individual laminae have been widely regarded as seasonal deposits (e.g., Chafetz et al., 1991). The actual mechanisms responsible for the layering of tufas, however, are relatively poorly understood, and can be different for individual cases. It has been conjectured that in some instances lamination is a result of seasonal differences in precipitation rate, whereas in others, it is due to the growth of different microbial species during different seasons. The latter appears to generate the layering observed in the present sample (Fig. 2). Electron microscopy indicates that flat-lying microbes cause the growth of thin, continuous layers, whereas upright microbes give rise to the columnar structures building up the thick layers. Because the sample was collected in July, during the dry season, the columnar growth habit of the outermost layer implies that thick laminae are probably dry season precipitates. According to the findings of Chafetz et al. (1991), a couplet comprising a thin and a thick layer is assumed to represent one annual cycle. Vertical lines in Figure 3 mark the limits of consecutive annual couplets. The lines are solid in cases where a thin, continuous layer is clearly developed, and dashed where it is less defined. By using these varve-like stratigraphic time markers, we find that the sampled section comprises ~14 annual cycles, thus representing the period from 1985 to 1999.

However, unless the driving mechanisms responsible for the observed lamination are fully understood, the accuracy and precision of this time frame cannot be assessed. Another stumbling block lies in developing a reliable intra-annual time series, because the exact time intervals represented by the thin and thick layers are not known. This uncertainty becomes particularly evident in the highly variable development of the thin, continuous layers. Furthermore, the extension rate of the tufa is presumed to wax and wane over the course of a year due to its close relation to the saturation state of calcite in the river water (Merz-Preiss and Riding, 1999).

#### 4.1.2. Water Temperature Chronometer

Considering the outlined shortcomings of this stratigraphic approach, we attempted to establish an independent timescale. Given the temperature dependence of the oxygen isotope fractionation between calcite and water, and the seasonal temperature variation of the river water, the  $\delta^{18}\text{O}$  fluctuations recorded in the tufa represent a potentially useful chronometer.

The  $\delta^{18}\text{O}$  value measured in a tufa sample reflects both temperature and the isotopic composition of the ambient water at the time of deposition. Therefore, it is not possible to ascribe the observed  $\delta^{18}\text{O}$  variations to temperature changes alone. The relationship existing between  $\delta^{18}\text{O}$  and Mg provides additional information, however, with which to further constrain the meaning of the oxygen isotope data. Like the oxygen isotope fractionation coefficient, the Mg partitioning between calcite and water varies with temperature. In contrast to the inverse temperature dependence of the oxygen isotope fractionation, the latter increases with rising temperature (e.g., O'Neil et al., 1969; Huang and Fairchild, 2001). Therefore, the anticorrelation between  $\delta^{18}\text{O}$  and Mg suggests that variation in both variables is indeed dominated by temperature fluctuations. Temporal changes in  $\delta^{18}\text{O}_{\text{rain}}$  and evaporative enrichment, on the other hand, cannot account for the observed anticorrelation, and thus seem to be of secondary importance. In regions characterized by a monsoon climate, such as the study area,  $\delta^{18}\text{O}_{\text{rain}}$  is often inversely related to the rainfall amount (e.g., Rozanski et al., 1993), as is groundwater residence time, which in turn may control the Mg/Ca ratio of karst waters (e.g., Fairchild et al., 2000). Depending on the strength of these interrelations, the records of  $\delta^{18}\text{O}$  and Mg would be either positively correlated or unrelated if variations in  $\delta^{18}\text{O}_{\text{rain}}$  were the main cause of the  $\delta^{18}\text{O}$  oscillation in the tufa. Likewise, evaporation would result in covarying or unrelated trends because it raises  $\delta^{18}\text{O}_{\text{water}}$  and, if calcite precipitation is triggered or enhanced, also increases  $(\text{Mg}/\text{Ca})_{\text{water}}$ .

Presuming that the  $\delta^{18}\text{O}$  oscillation in the tufa mainly reflects variations in water temperature, it is now possible to establish a timescale for the sampled profile by matching the wavelengths of the oxygen isotope and water temperature records. The result of this step is illustrated in Figure 4. The  $\delta^{18}\text{O}$  data of the tufa are converted to equivalent temperature values using the coefficients given by O'Neil et al. (1969) and a  $\delta^{18}\text{O}_{\text{water}}$  of  $-7.64\text{‰}$ . The latter was estimated from the  $\delta^{18}\text{O}$  of the outermost sample (GMT-1) assuming a water temperature of  $25.6^\circ\text{C}$ , the average observed water temperature during the time from the onset of the dry season (end of March) to mid-July. Sample GMT-1 is surmised to cover

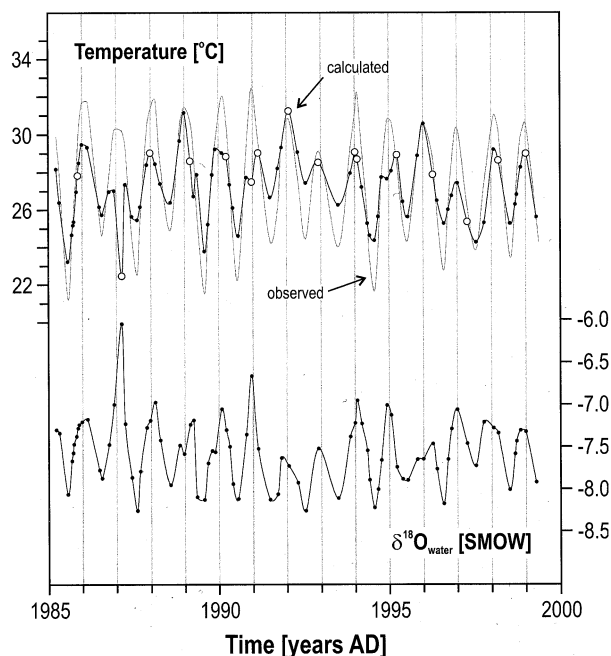


Fig. 4. (top) Calculated  $\delta^{18}\text{O}$  temperatures for the tufa profile superimposed on the observed water temperature cycle. The  $\delta^{18}\text{O}$  temperatures were determined using the coefficients given by O'Neil et al. (1969) and assuming a constant  $\delta^{18}\text{O}_{\text{water}}$  of  $-7.64\text{‰}$  (SMOW). Water temperatures are modeled from the composite air temperature record (see section 1.2), and time-averaged corresponding to the variable temporal resolution of the tufa samples, to enable a direct comparison with the calculated temperatures. The time series for the tufa record was developed by matching the wavelengths of the calculated and observed temperature oscillations. Open symbols indicate samples from thin, continuous layers (see Fig. 2). Deposition of these layers appears to be restricted to the annual wet season, implying a seasonal control on their formation. (bottom) Temporal variation of  $\delta^{18}\text{O}_{\text{water}}$  as calculated by removing the temperature component of the measured  $\delta^{18}\text{O}_{\text{tufa}}$  values. Note the pronounced seasonality of the variation. See sections 1.2, 4.1, and 4.2 for discussion.

this period because of its columnar growth habit, which indicates dry season deposition. The good agreement between the calculated  $\delta^{18}\text{O}_{\text{water}}$  and the measured  $\delta^{18}\text{O}$  of the water sample collected in July 1999 ( $-7.87\text{‰}$ ; Table 1) supports our previous assumption that the oxygen isotope fractionation between the tufa and water occurred under near-equilibrium conditions. The water temperature record shown in Figure 4 is time-averaged in accordance with the variable temporal resolution of the tufa samples, to enable a direct comparison of the two records.

According to the isotope-based timescale, the period from early 1985 to July 1999 is covered by the tufa profile (Fig. 4), which is in excellent agreement with the stratigraphically defined chronology described in section 4.1.1. It is therefore evident that couplets comprising a thin and a thick layer represent annual cycles, as previously speculated. Furthermore, the seasonal nature of individual laminae appears to be confirmed because thin, continuous layers are generally developed around the turn of the year during the annual wet season (Fig. 4). The overall accuracy of the isotope-based timescale is supported by the agreement between the two independent chronologies. Its precision, however, is difficult

to quantify since it is mainly defined by uncertainties in the underlying assumptions, such as the temperature control of  $\delta^{18}\text{O}$  variations. We surmise that the precision of the time-scale is probably on the order of the temporal resolution of individual samples. The latter averages  $\sim 2.1$  months, but varies along the profile depending on the tufa extension rate, which ranges from  $0.50 \text{ cm yr}^{-1}$  ( $19 \text{ nmol cm}^{-2} \text{ min}^{-1}$ ) in 1993 to  $0.95 \text{ cm yr}^{-1}$  ( $36 \text{ nmol cm}^{-2} \text{ min}^{-1}$ ) in 1985. The overall mean for the entire record is  $0.65 \text{ cm yr}^{-1}$  ( $25 \text{ nmol cm}^{-2} \text{ min}^{-1}$ ).

#### 4.2. The $\delta^{18}\text{O}$ Record

The average  $\delta^{18}\text{O}$  temperature of all 83 samples ( $27.2^\circ\text{C}$ ) is in fairly good agreement with the mean water temperature during the corresponding period ( $27.7^\circ\text{C}$ ), thereby suggesting that the estimated  $\delta^{18}\text{O}$  value of the water is a reasonably good approximation of the actual isotope composition. The seasonal amplitude of the calculated temperature variation, however, is markedly smaller than that of the observed water temperatures (Fig. 4). Because the time resolutions of the two records were adjusted, smoothing of the tufa signal due to time-averaging cannot account for these deviations. The subdued amplitude of the calculated temperatures therefore indicates temporal changes in the oxygen isotope composition of the ambient water.

In order to reveal the nature of this variation, we removed the temperature component of the  $\delta^{18}\text{O}_{\text{tufa}}$  signal. The resulting pattern suggests a fairly regular, seasonal fluctuation in the oxygen isotope composition of the river water (Fig. 4).  $\delta^{18}\text{O}$  values are systematically higher during the austral summer (mean maximum:  $-7.1 \pm 0.4\text{‰}$ ,  $1\sigma$ ) than during the winter (mean minimum:  $-8.1 \pm 0.2\text{‰}$ ,  $1\sigma$ ), resulting in an average seasonal amplitude of  $\sim 1\text{‰}$ . Apparently, the  $\delta^{18}\text{O}$  temperature depression in 1987 is due to a relatively extreme isotope enrichment of the water, which is not erratic but part of an annual cycle (Fig. 4).

Since precipitation is almost exclusively restricted to the wet season, seasonal variations in rainfall composition cannot account for the observed isotopic fluctuations of the river water. Hydrological processes occurring in the karst aquifer could be responsible instead. The isotopic characteristics of rainfall-recharge relationships within a karstic terrain in a semiarid region were investigated by Ayalon et al. (1998). Their study revealed that  $\delta^{18}\text{O}$  values of slow-drip cave waters are systematically higher (by  $\sim 0.5$  to  $1.5\text{‰}$ ) than that of fast-drip waters. The distinct isotopic compositions of the two water-types are thought to arise mainly from different modes of water incorporation in the soil and upper vadose zone. Applying these findings to the present case, we would expect increasing  $\delta^{18}\text{O}$  values in the river water toward the end of the rainy season and during the dry season, as a result of a gradually diminishing contribution of isotopically lighter, high-velocity conduit flow (i.e., fast drip waters) to the discharge of the Gregory River. This expected trend, however, is in stark contrast to the observed pattern. Therefore, the seasonal fluctuations must have another cause.

We propose instead that the varying  $^{18}\text{O}$  enrichment of the river water is driven by seasonal differences in evaporation from the water surface. The mean daily evaporation observed at

the six weather stations surrounding the study area shows a clear seasonal trend supporting our interpretation. Over the course of a year, the highest evaporation generally occurs from October to December ( $\sim 10.8 \text{ mm/day}$ ), the lowest from May to July ( $\sim 5.9 \text{ mm/day}$ ). By using the ratio of 1.8 between mean evaporation rates for October to December and May to July, combined with the previously calculated summer/winter  $\delta^{18}\text{O}_{\text{water}}$  averages of  $-7.1\text{‰}$  and  $-8.1\text{‰}$  respectively, the average evaporative loss during summer/winter and the mean  $\delta^{18}\text{O}$  of “pristine” spring water can be estimated from Rayleigh fractionation calculations. Kinetic fractionation factors, calculated for the respective humidities using the relationship given by Gonfiantini (1986), were included in these calculations. The latter indicate that the average water loss due to evaporation along the river from the springs to the sampling site ranges from  $\sim 7\%$  in winter to  $\sim 12\%$  in summer. The average  $\delta^{18}\text{O}$  of water unaffected by evaporation is calculated as  $-9.2\text{‰}$  (SMOW). These estimates agree well with  $\delta^{18}\text{O}$  and chloride data measured along downstream traverses in nearby Louie Creek, another tufa-depositing stream draining the same karst aquifer (Drysdale, unpublished data). In December 1996, the  $\delta^{18}\text{O}$  of Louie Creek waters increased systematically from  $-8.5\text{‰}$  (SMOW) near its origin to  $-6.6\text{‰}$  (SMOW) 13 km downstream, corresponding to an evaporative loss of  $\sim 11\%$ . Chloride concentrations along the same stretch of Louie Creek rose steadily from 152 to 190  $\mu\text{mole/L}$  in October 1993 ( $\sim 25\%$  enrichment), and from 243 to 264  $\mu\text{mole/L}$  in April 1994 ( $\sim 9\%$  enrichment), thereby confirming the seasonal difference in downstream enrichment. We conclude, therefore, that the inferred  $\delta^{18}\text{O}_{\text{water}}$  variations shown in Figure 4 are most likely related to seasonally variable evaporation rates.

#### 4.3. Mg Thermometry: A Bright Spot on the Horizon?

While the partitioning of Mg between calcite and water is potentially controlled by a number of factors (e.g., Mucci and Morse, 1983; Zhong and Mucci, 1989; Burton and Walter, 1991), the only relevant influence in solutions with low ionic strength and low Mg/Ca ratios ( $\leq 1$ ) is thought to be temperature (e.g., Huang and Fairchild, 2001). In the vast majority of freshwater environments, the Mg content of calcite precipitates is therefore solely determined by the Mg/Ca ratio and the temperature of the parent solution. Over the last two decades several studies on cave deposits have attempted to exploit this temperature dependence as a paleothermometer (e.g., Goede, 1994; Roberts et al., 1998, 1999). However, all these approaches clearly demonstrate that temporal variations in the Mg/Ca ratios of the cave waters confounded or even completely disguised any existing relationship between temperature and the speleothems' Mg content. It is not surprising, though, that Mg records of speleothems primarily reflect changes in water chemistry. While temperatures in cave interiors are fairly constant over periods of up to decades, the Mg/Ca ratio of seepage waters is known to vary on a much shorter timescale (e.g., Fairchild et al., 2000).

In contrast to the nearly isothermal conditions in enclosed caves, the water temperature of the Gregory River oscillates seasonally by  $\sim 10^\circ\text{C}$ . Due to this large short-term variability, seasonal changes in Mg content within the present sample are temperature dominated, as outlined in section 4.1.2. Using the

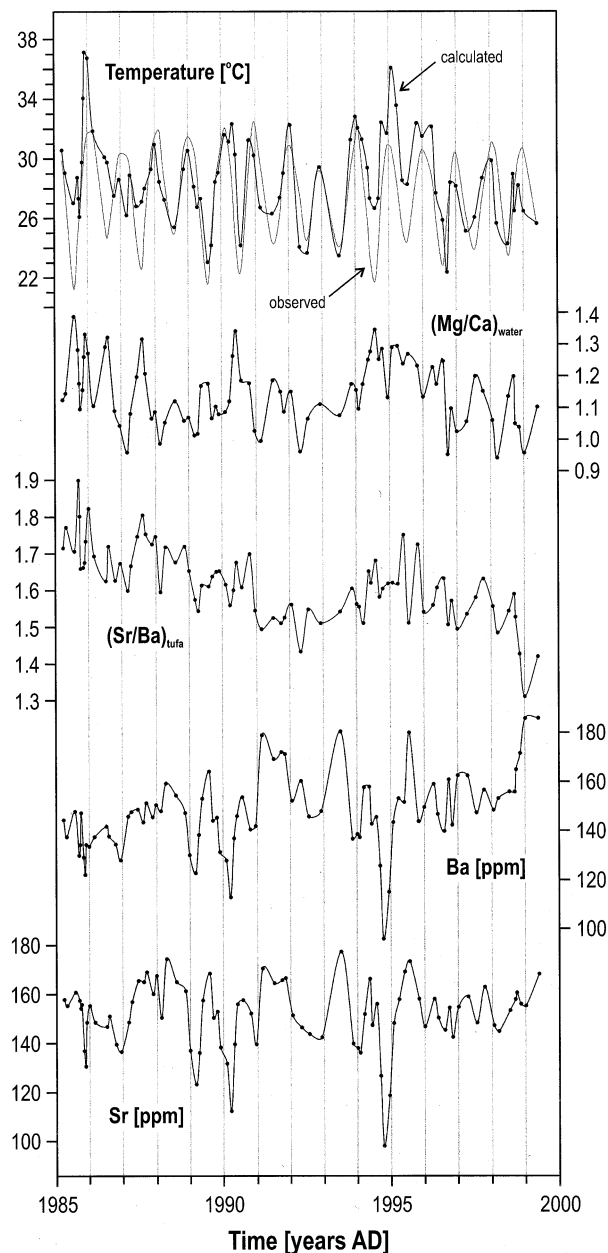


Fig. 5. (top panel) Model temperatures, calculated from the measured Mg concentrations using the  $D_{Mg}$ - $T$  relationship given by Huang and Fairchild (2001) and assuming a constant atomic  $(Mg/Ca)_{water}$  of 1.102, superimposed on the observed water temperature cycle (see caption to Fig. 4 and section 1.2). The temporal variation of the atomic  $(Mg/Ca)_{water}$  (second panel from top) was determined by removing the temperature component of the measured Mg concentrations.  $(Mg/Ca)_{water}$  is clearly correlated with the atomic  $(Sr/Ba)_{tufa}$  (third panel from top), which offers the possibility to estimate the Mg/Ca ratio of paleowaters from Sr and Ba concentrations measured in fossil tufas. The patterns of Ba and Sr (bottom panels) are shown for comparison. See section 4.3 for discussion.

relationship between the Mg distribution coefficient ( $D_{Mg}$ ) and temperature ( $T$ , °C) obtained by Huang and Fairchild (2001), and assuming a  $(Mg/Ca)_{water}$  of 1.102 (see below), we calculated model temperatures from the Mg concentrations of the

tufa samples (Fig. 5). The choice of this particular  $D_{Mg}$ - $T$  relationship appears to be appropriate because it was determined for calcite precipitation from solutions of low ionic strength under controlled, karst-analog experimental conditions. In contrast,  $D_{Mg}$ - $T$  relationships of other authors are considered to be less robust (Gascoyne, 1983; Oomori et al., 1987) or not applicable to the freshwater environment of the Gregory River (e.g., Mucci, 1987; Burton and Walter, 1991), for reasons discussed by Huang and Fairchild (2001). The  $(Mg/Ca)_{water}$  of 1.102 was estimated from the Mg/Ca of the outermost tufa sample assuming a water temperature of 25.6°C (analogous to  $\delta^{18}O$ ; section 4.1.2), and compares well with the measured Mg/Ca ratio of the water sample collected in July 1999 (1.028; Table 1). This agreement, as well as the fairly good match between the calculated and observed water temperatures ( $r = 0.61$ ), especially during the period from 1988 to 1994 ( $r = 0.78$ ), indicate the general validity of our approach.

Assuming that the Mg content of tufa solely depends on temperature and the  $(Mg/Ca)_{water}$  ratio, we can ascribe deviations of the calculated temperatures from the observed values (e.g., 1985 to 1987, 1994 to 1996) to changes in  $(Mg/Ca)_{water}$ . To quantify these changes, we removed the temperature component of the Mg signal (Fig. 5). The calculated  $(Mg/Ca)_{water}$  values (0.94 to 1.39) straddle the upper limit of the range for which  $D_{Mg}$  is shown to be unaffected by variations in  $(Mg/Ca)_{water}$  (0.15 to 1.0; Howson et al., 1987). Therefore, a potential influence of changing  $(Mg/Ca)_{water}$  on  $D_{Mg}$  cannot be ruled out completely (Mucci and Morse, 1983). However, as estimated from the experimental data of Mucci and Morse (1983), the potential changes in  $D_{Mg}$  would be relatively small ( $\sim 0$  to 5%) in the present case, and would therefore not seriously compromise our approach.

Compared with  $\delta^{18}O_{water}$  (Fig. 4), the seasonality of the  $(Mg/Ca)_{water}$  variation is less conspicuous and longer-term trends are more pronounced. Nonetheless, values are generally higher during the dry season than during the wet season. Remarkably,  $(Mg/Ca)_{water}$  ratios are significantly larger than Mg/Ca ratios of bedrock carbonates from the Gregory River catchment (Table 2). To explain this enhancement, processes such as calcite precipitation along the flow path of the water (see sections 4.4.1 and 4.4.2), and/or selective leaching of Mg with respect to Ca during bedrock weathering (Fairchild et al., 2000) need to be invoked. Fluctuations in the degree of these processes could cause at least some of the temporal variations in  $(Mg/Ca)_{water}$ . The latter may also arise from shifts in the relative contribution of waters from the dolomite and limestone lithologies of the catchment, or from changes in the groundwater residence time. Due to the differential dissolution kinetics of dolomite and calcite, water residence time in mixed dolomite–limestone karst aquifers is thought to be one of the key factors controlling  $(Mg/Ca)_{water}$  (e.g., Roberts et al., 1998; Fairchild et al., 2000). As water–rock contact times are increased during drier conditions, dolomite dissolution is enhanced relative to calcite dissolution, leading to higher  $(Mg/Ca)_{water}$  (e.g., Fairchild et al., 2000). Since dolomite in the Gregory River catchment generally has lower Sr/Ca and Ba/Ca than calcite (Table 2), increasing  $(Mg/Ca)_{water}$  ratios in response to enhanced dolomite dissolution, or to an increased contribution from the dolomite lithology, are likely to be matched by decreasing  $(Sr/Ca)_{water}$  and  $(Ba/Ca)_{water}$ , and hence

decreasing Sr-Ba concentrations in the tufa. As can be seen in Figure 5, Ba shows longer-term trends which tend to mirror the temporal evolution of  $(\text{Mg}/\text{Ca})_{\text{water}}$ , whereas Sr is more or less invariable on a longer timescale, despite its striking short-term covariation with Ba. Normalizing the Ba concentration to Sr thus emphasizes the long-term trend of the Ba signal by removing most of its shorter-term fluctuations. The temporal variation of the  $(\text{Sr}/\text{Ba})_{\text{tufa}}$  ratio, the reciprocal of the Sr-normalized Ba concentration, is shown in Figure 5.  $(\text{Mg}/\text{Ca})_{\text{water}}$  and  $(\text{Sr}/\text{Ba})_{\text{tufa}}$  are significantly correlated ( $r = 0.50$ ), as reflected in the correspondence of their longer-term trends and some of their annual/seasonal features. The relationship between the atomic  $(\text{Mg}/\text{Ca})_{\text{water}}$  and  $(\text{Sr}/\text{Ba})_{\text{tufa}}$  ratios is described by the following linear equation:

$$(\text{Mg}/\text{Ca})_{\text{water}} = 0.526 (\text{Sr}/\text{Ba})_{\text{tufa}} - 0.296. \quad (1)$$

By means of this relation it is potentially possible to derive the approximate Mg/Ca ratio of paleowaters from the concentrations of Sr and Ba measured in fossil tufas, and consequently feasible to reliably estimate former water temperatures. To test the adequacy of this approach, we calculated  $(\text{Mg}/\text{Ca})_{\text{water}}$  ratios from the  $(\text{Sr}/\text{Ba})_{\text{tufa}}$  ratio of each sample using the above equation, and inserted the obtained values to calculate Mg model temperatures for the data set. The resulting pattern shows a remarkable synchronism with the observed water temperature oscillation ( $r = 0.69$ ). The difference between individual model temperatures and the actual values is  $-0.1 \pm 2.2^\circ\text{C}$  ( $1\sigma$ ). Despite some deviations in detail, the average summer maximum ( $30.8^\circ\text{C}$ ) and the average winter minimum ( $24.1^\circ\text{C}$ ) of the calculated temperatures are in excellent agreement with the corresponding values of the time-averaged water temperature record ( $31.1^\circ\text{C}$  and  $23.3^\circ\text{C}$ , respectively).

We therefore conclude that the relationship between  $(\text{Mg}/\text{Ca})_{\text{water}}$  and  $(\text{Sr}/\text{Ba})_{\text{tufa}}$  is adequate to reliably estimate changes in the Mg/Ca ratio of the river water. A successful application of the proposed approach to fossil tufas requires, however, that the same processes which controlled the Mg/Ca and Sr/Ba variations during the period covered by the present sample also govern on longer timescales. Considering that unknown temporal variations in the Mg/Ca ratio of parent waters have been an almost insurmountable obstacle in deriving temperatures from the Mg content of terrestrial carbonates, our findings represent a promising advance. While the correlation between  $(\text{Mg}/\text{Ca})_{\text{water}}$  and  $(\text{Sr}/\text{Ba})_{\text{tufa}}$ , described above, applies only to the catchment of the Gregory River, it is likely that similar relationships exist in other karst environments. Further investigation of these relationships will help to fully exploit the potential of Mg thermometry in the future.

#### 4.4. Sr, Ba, and $\delta^{13}\text{C}$ : Delayed Messengers of Rainfall Intensity

Variations in Sr and Ba concentrations within speleothems have been found in a considerable number of studies, and the processes invoked to explain these temporal changes are almost as numerous (e.g., Goede et al., 1998; Roberts et al., 1998, 1999; Ayalon et al., 1999; Hellstrom and McCulloch, 2000). The diversity of the various explanatory models reflects the multitude of potential causes, and highlights that different mechanisms may prevail at individual sites. Furthermore, it is

probable that distinct processes control the chemistry of fresh-water carbonates on different timescales. As will be discussed below, the variations in Sr and Ba in the present sample (Fig. 6) may in principle arise from changes in variables influencing the partitioning of these elements during calcite precipitation, and/or fluctuations in the Sr/Ca and Ba/Ca ratios of the parent waters.

##### 4.4.1. Constraining the Relevant Geochemical Processes

Experimental studies have shown that the Sr distribution coefficient between calcite and water may be influenced by the

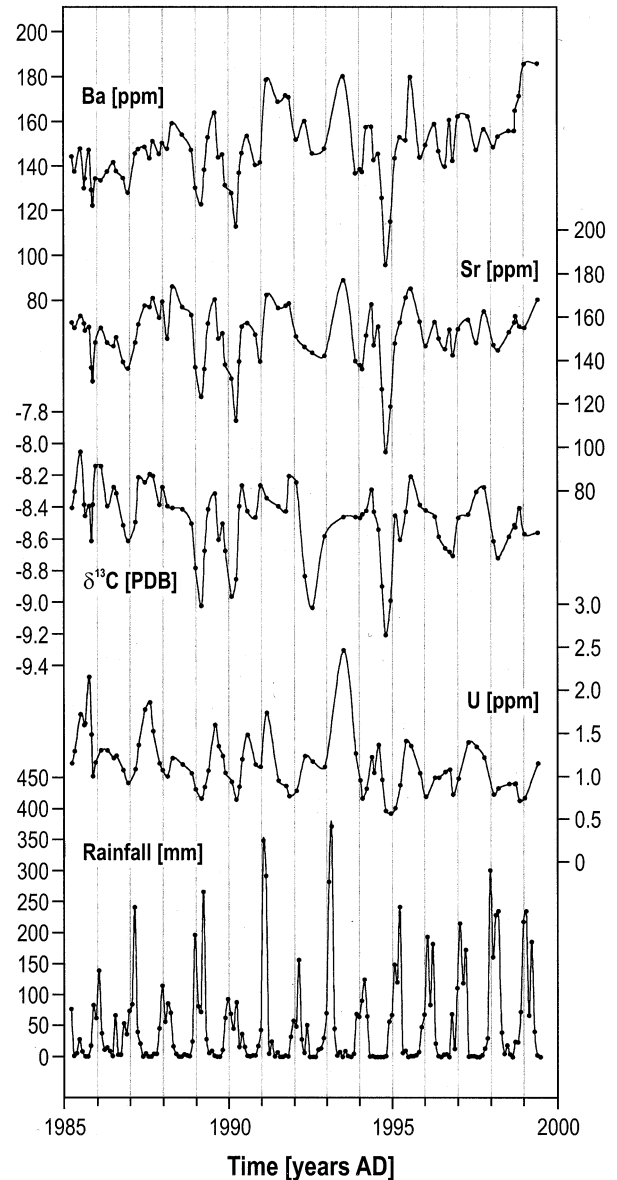


Fig. 6. Comparison of temporal variations in Ba, Sr,  $\delta^{13}\text{C}$ , and U along the sampled tufa profile with the composite rainfall record (see section 1.2). Negative spikes in the patterns of Ba, Sr, and  $\delta^{13}\text{C}$  are thought to be related to "wet" rainy seasons. Due to the water residence time in the karst aquifer, the Ba, Sr, and  $\delta^{13}\text{C}$  signals in the tufa lag the rainfall events by 1 to 2 yr. Note the resemblance between the U record and the biennial rainfall cycle. See sections 4.4 and 4.5 for discussion.

Table 2. Composition of bedrocks from the Gregory River catchment.

Element	Limestones <sup>a</sup> (n = 3)	Dolomites (n = 2)	Siliciclastics <sup>a</sup> (n = 34)
			(Mean ± $\sigma$ )
		Concentrations	
Mg (%)	2.9, 2.0, 1.6	10.6, 10.1	0.6 ± 0.3
Ca (%)	30.4, 31.0, 30.3	23.4, 20.3	1.1 ± 0.5
Sr (ppm)	275, 210, 300	36, 32	33 ± 10
Ba (ppm)	2029 <sup>b</sup> , 2817 <sup>b</sup> , 87	3.2, 1.6	255 ± 110
U (ppm)	8.5, 4.0, 1.5	0.14, 0.08	2.6 ± 1.2
		Atomic ratios	
Mg/Ca	0.08–0.16	0.75–0.82	1.02 ± 0.21
Sr/Ca	3.1–4.5 ( $\times 10^{-4}$ )	7.0–7.2 ( $\times 10^{-5}$ )	1.660.6 ( $\times 10^{-3}$ )
Ba/Ca	0.08–2.7 ( $\times 10^{-3}$ )	2.3–4.0 ( $\times 10^{-6}$ )	7.663.5 ( $\times 10^{-3}$ )
U/Ca	0.8–4.7 ( $\times 10^{-6}$ )	6.7–9.9 ( $\times 10^{-8}$ )	4.863.0 ( $\times 10^{-5}$ )

<sup>a</sup> Data from the OZCHEM database (Budd et al., 2000).

<sup>b</sup> Sample contains baryte (P. N. Southgate, AGSO, personal communication).

concentrations of competing cations (e.g., Na and Ba) in the solution, its Sr/Ca ratio (Pingitore and Eastman, 1986), the Mg content of the precipitate (Mucci and Morse, 1983), and the calcite precipitation rate (e.g., Lorens, 1981; Tesoriero and Pankow, 1996; Huang and Fairchild, 2001). While a growth rate dependence is also demonstrated for the Ba distribution coefficient (e.g., Tesoriero and Pankow, 1996), the effects of solution composition and/or Mg content on Ba partitioning have not been examined. It is likely, however, that these factors influence the incorporation of Ba in a way similar to Sr (Mucci and Morse, 1983; Pingitore and Eastman, 1986).

Changes in the calcite precipitation rate, considered the key variable influencing Sr and Ba partitioning by several workers (e.g., Lorens, 1981; Tesoriero and Pankow, 1996; Huang and Fairchild, 2001), probably account for some of the Sr and Ba fluctuations, given the relatively high and variable growth rate of the tufa sample (19 to 36 nmol cm<sup>-2</sup> min<sup>-1</sup>). In addition, temporal changes in the other factors, such as the pronounced variation in Mg content along the sampled profile (Fig. 3), may have also modulated Sr and Ba incorporation to some extent. Overall, however, variations in the distribution coefficients must be of secondary importance in causing the Sr and Ba concentration changes because they cannot account for the strong correlation of Sr and Ba with  $\delta^{13}\text{C}$ . Carbon isotope fractionation between calcite and bicarbonate has been shown to be insensitive to variations in precipitation rate and temperature (Romanek et al., 1992), and is not known to be influenced by any of the other factors mentioned above. In line with this reasoning, the Sr and Ba concentrations of the tufa are unrelated to the observed changes in calcite precipitation rate (shown by the variable thickness of annual growth layers), and do not covary with the Mg content (Fig. 3). We therefore conclude that the variations in Sr and Ba recorded in the tufa primarily reflect temporal changes in the Sr/Ca and Ba/Ca ratios of the river water.

As outlined in section 4.3, differential dissolution of dolomite and calcite in response to changing water residence time in the karst, and/or shifts in the relative contributions of water from the dolomite and limestone lithologies, are probably responsible for some of the variability in (Sr/Ca)<sub>water</sub> and (Ba/Ca)<sub>water</sub>. However, since none of the pronounced Sr-Ba minima of the tufa record coincides with an equivalent maximum in

(Mg/Ca)<sub>water</sub> (Fig. 5), neither of these two processes can be the primary cause.

Fluctuations in the Sr/Ca and Ba/Ca ratios of the Gregory River water could also be related to temporal variations in the relative fluxes of Sr, Ba, and Ca from the soil zone to the water table. Such variations may occur, but seem to be of minor significance in the present case, because Sr and Ba are strongly correlated along the entire tufa profile despite their markedly different mobilities in soils (e.g., Nesbitt et al., 1980; McBride, 1994).

In some cases, temporal changes in the Sr/Ca ratio of karst waters have been attributed to variable degrees of selective Sr release during CaCO<sub>3</sub> weathering (e.g., Fairchild et al., 2000). Such incongruent effects are mainly known from young carbonate aquifers (e.g., Reeve and Perry, 1994) where transformation of one CaCO<sub>3</sub>-phase to another occurs (e.g., aragonite to calcite), but have also been observed in leaching experiments on pure calcites (Fairchild et al., 2000). However, like all the other processes described so far, selective leaching cannot readily account for the strong correlation of Sr-Ba with  $\delta^{13}\text{C}$  in the tufa, and is therefore probably of secondary importance in the present case.

Variable contributions of water from the silicate lithology to the Gregory River can also be dismissed as a significant mechanism, as follows. The  $\delta^{13}\text{C}$  of the soil CO<sub>2</sub> in the catchment lies probably between about -26‰ and -18‰, depending on the actual proportions of C<sub>3</sub> (trees, shrubs) and C<sub>4</sub> (grasses) plants contributing to the soil gas. The lower limit of this range is based on published data for C<sub>3</sub> plants (Vogel, 1993), including a diffusive enrichment of ~4‰ (Cerling et al., 1991), whereas the upper limit is estimated from the lowest  $\delta^{13}\text{C}$  value measured in the tufa sample. While the  $\delta^{13}\text{C}$  of waters derived from the Proterozoic silicates reflects primarily the composition of the soil CO<sub>2</sub>, the  $\delta^{13}\text{C}$  of the karst waters evolves to more enriched values as isotopically heavy carbonate is dissolved. The  $\delta^{13}\text{C}$  of the Cambrian carbonates in the catchment of the Gregory River is assumed to lie between -2‰ and 1‰ (e.g., Veizer et al., 1999). Therefore, waters draining the karst have higher  $\delta^{13}\text{C}$  values than waters discharging from the silicate lithology. On the other hand, Sr/Ca and Ba/Ca ratios of waters derived from the carbonate rocks of the catchment are most probably smaller than those of waters draining the silicates

(Table 2). Hence, variations in the proportions of waters derived from the silicate and carbonate rocks in the catchment would result in antithetic trends of  $\delta^{13}\text{C}$  and Sr-Ba in the tufa.

On the basis of this reasoning, we infer that the only process capable of generating the sympathetic Sr, Ba, and  $\delta^{13}\text{C}$  patterns in the present sample is calcite precipitation along the flow path of the parent water. Karstic waters typically become supersaturated with respect to calcite when allowed to equilibrate by degassing with an atmosphere with lower  $p\text{CO}_2$  than that of the soil. Consequently, the system tends to re-establish the chemical equilibrium by precipitation of calcite according to the following equation:  $\text{Ca}^{2+} + 2\text{HCO}_3^- \rightarrow \text{CaCO}_3 \downarrow + \text{CO}_2 \uparrow + \text{H}_2\text{O}$ . As calcite precipitation occurs, dissolved bicarbonate is equally fractionated into two phases, calcium carbonate and  $\text{CO}_2$ , resulting in an overall isotopic enrichment of the carbon remaining in solution (Mook et al., 1974; Romanek et al., 1992). This increase in  $\delta^{13}\text{C}$  is accompanied by a rise in the Sr/Ca and Ba/Ca ratios of the water, because partitioning coefficients for both Sr and Ba are  $\ll 1$  (e.g., Tesoriero and Pankow, 1996).

To test whether the observed variations are quantitatively compatible with the proposed model, we carried out a Rayleigh fractionation calculation for the major fluctuation in Sr, Ba, and  $\delta^{13}\text{C}$  in 1994/95 (Fig. 6). Assuming that the absolute minima in late 1994 (sample GMT-25) reflect the composition of water that has not experienced prior calcite precipitation, we calculated the fraction of Ca and C which needs to be removed from the system, to drive the composition to the maximum values in mid-1995 (sample GMT-20). To yield the observed changes,  $\sim 47\%$  of the initially dissolved Ca, and  $\sim 29\%$  of the C have to be fractionated. For each mole of Ca, two moles of C are withdrawn from the solution as  $\text{CaCO}_3$  precipitates. Thus, to be consistent with the model, the carbon pool needs to be  $\sim 3.2$  times as large as the calcium pool, which is in good agreement with the molar ( $\text{HCO}_3^-/\text{Ca}$ ) ratio of 3.4 determined for the river water in July 1999 (Table 1). We therefore conclude that calcite precipitation along the flow path of the parent water is a reasonable explanation for the covariations between Sr, Ba, and  $\delta^{13}\text{C}$ . As indicated by the data in Drysdale et al. (2002), the amount of calcite precipitation along the Gregory River upstream of the sample location (station G11 of Drysdale et al.) is only on the order of  $10^{-2}$  mmole/L. Hence, most of the inferred calcite precipitation must occur in the vadose zone of the karst aquifer.

Occasionally, the correlation between  $\delta^{13}\text{C}$  and Sr-Ba wanes, as most obvious in 1992/93 and 1996/97 (Fig. 6), suggesting that sometimes other processes gain importance. During these periods of weakened correlation, Sr and Ba concentrations are generally enriched compared with the corresponding  $\delta^{13}\text{C}$  values. Therefore, this temporary decoupling could be related to increased Sr and Ba partition coefficients, enhanced fluxes of Sr and Ba from the soil to the water table, selective leaching of these elements during carbonate dissolution, or to an increased contribution of waters from the silicate lithology (see above). Since Sr is derived from sources that should be isotopically distinct (i.e., soil, Cambrian carbonates and Proterozoic silicates), a supplementary Sr isotope study of the tufa sample may help to clarify this issue. On the other hand,  $\delta^{13}\text{C}$  values could be lowered without corresponding decreases in Sr and Ba, if carbonate dissolution temporarily

occurs under increasingly open system conditions (e.g., Hendy, 1971). While respiration and decomposition of organic matter in the river can likewise explain lighter  $\delta^{13}\text{C}$  values in the water, in situ photosynthesis would drive the isotopic composition toward heavier values (e.g., Andrews et al., 1997), and can therefore be ruled out as a relevant process.

#### 4.4.2. Link between Chemistry and Climate

In line with the goal of our study, a major question is whether the annual and seasonal fluctuations in Sr, Ba, and  $\delta^{13}\text{C}$  can be related to changes in climate conditions. If the observed covariations are mainly controlled by calcite precipitation within the karst aquifer, as proposed in the previous section, this could be done in a relatively simple way. Since calcite precipitation along the flow path is triggered by  $\text{CO}_2$  degassing of the water into air pockets etc., it could be enhanced during periods of decreased recharge, when the water saturation in the vadose zone is low. Conversely, low Sr, Ba, and  $\delta^{13}\text{C}$  values in the tufa should correspond to periods of high rainfall, when degassing is suppressed as a result of high water saturation in the epikarst. To check this model, we compare the amount of precipitation in the study area with the patterns of Sr, Ba, and  $\delta^{13}\text{C}$  (Fig. 6). While the highest rainfall within the period covered by the tufa sample occurred during the wet season 1992/93, the lowest Sr, Ba, and  $\delta^{13}\text{C}$  values are observed almost 2 yr later, just before the wet season 1994/95. Rainfall in 1993/94 was well below average and therefore cannot account for the observed minima according to the proposed model. To reconcile the precipitation and tufa records, a time lag between the rainfall peak and the related chemical signature has to be postulated. The apparent lag could readily be explained by the residence time of the groundwater in the karst aquifer. Hydrograph separations of discharge from karst springs have shown that most of the recharging rainwater does not contribute to discharge immediately after the rain event, but is stored in the aquifer for variable periods. Even during peak flow conditions after rainstorms the bulk of discharge is derived from groundwater storage (e.g., Rank et al., 1992; Lakey and Krothe, 1996). This implies that stored water is displaced by the infiltrating rain and flushed out as a result of increased hydraulic heads. The residence time of waters is not uniform throughout a karst aquifer, but varies for the different storage compartments. While groundwater can be stored in small-scale fissures and the porous matrix of karst aquifers for periods from a few years up to several decades (e.g., Even et al., 1986; Rank et al., 1992), the larger conduits have mean transit times of less than 1 yr (e.g., Rank et al., 1992; Ayalon et al., 1998).

If water storage in the karst is the actual reason for the apparent mismatch between the precipitation and the tufa record, the Sr, Ba, and  $\delta^{13}\text{C}$  signals related to other high rainfall events should be delayed by a similar period. The expected lag is indeed observed for the  $\delta^{13}\text{C}$  minimum in 1992, which follows the extraordinarily "wet" rainy season 1990/91 by  $\sim 1.5$  yr. As discussed earlier, the Sr and Ba records do not display equivalent minima in this specific case, due to processes which need to be further constrained by supplementary investigations. Nonetheless, the concentration of both elements decreases during the period in question. The minima in 1989 and 1990, synchronous in all three records, are most probably related to

the above-average rainfall during the wet seasons 1986/87 and 1988/89. This raises the question why the minima in the tufa record occur in two consecutive years, whereas the supposedly related rain events are 2 yr apart. One possible explanation for this mismatch is local rainfall variations in the area, which are not detected in the composite precipitation record shown in Figure 6. Another reason could be dispersive mixing of different water generations during groundwater storage in the karst aquifer. Assuming a mean water residence time of 1.5 yr, waters discharged in 1989 and 1990 may be composed of equal amounts of rainwater infiltrated during the wet seasons 1986/87, 1987/88 and 1987/88, 1988/89 respectively, thereby explaining Sr-Ba- $\delta^{13}\text{C}$  minima in two consecutive years (Fig. 6). The expected minima corresponding to the high rainfall during the wet season 1997/98 are not recorded in the tufa sample (collected in 1999), which would be consistent with the proposed water residence time of 1 to 2 yr.

Remarkably, conspicuous positive spikes corresponding to years of below-average rainfall are absent. This may imply that a fairly consistent enrichment of the waters in Sr/Ca, Ba/Ca, and  $\delta^{13}\text{C}$  due to prior calcite precipitation is the "normal" state in the karst aquifer during and after average or below-average wet seasons. Only if the amount of wet season rainfall exceeds a certain threshold ( $\sim 620$  to  $650$  mm),  $\text{CO}_2$  degassing of the water into air pockets etc. and hence calcite precipitation are significantly subdued, resulting in reduced trace element and isotope enrichment. This threshold may vary in response to factors influencing the infiltration of rainwater, such as the timing and volume of individual rain events.

An apparent shortcoming in our proposed calcite precipitation model is the lack of correlation between Sr-Ba- $\delta^{13}\text{C}$  and  $(\text{Mg}/\text{Ca})_{\text{water}}$ . Because the Mg calcite-water distribution coefficient is  $\ll 1$  (e.g., Mucci and Morse, 1983; Huang and Fairchild, 2001), the Mg/Ca ratio is expected to covary with Sr/Ca, Ba/Ca, and  $\delta^{13}\text{C}$ . However, none of the conspicuous minima discussed above is recorded in the  $(\text{Mg}/\text{Ca})_{\text{water}}$  pattern (Fig. 5). A possible reason for this could be the difference in the mass balances of the elements in question. While Sr, Ba, and C are derived from several geochemical reservoirs within the catchment, including both limestones and dolomites, Mg is almost exclusively supplied from waters draining the dolomite lithology. To explain the absence of pronounced minima in the  $(\text{Mg}/\text{Ca})_{\text{water}}$  pattern, we propose that even after high wet season rainfall calcite precipitation in the dolomite karst is not markedly subdued. The different chemical evolution of waters in the limestone and dolomite karsts may be related to distinct hydrogeological properties of the two aquifers.

While some details need to be explored further, the suggested model appears to be reasonably successful in relating the variations in Sr, Ba, and  $\delta^{13}\text{C}$  to changes in the amount of rainfall. Remarkably, the amplitudes of the negative anomalies in the three records are proportional to the cumulative rainfall during the supposedly reflected "wet" rainy seasons. Although the limitations of the data set do not allow an unambiguous definition of the transfer functions between the amount of rainfall and the chemical proxies, our results suggest a systematic relationship. The Sr, Ba, and  $\delta^{13}\text{C}$  records of fossil tufas, therefore, have the potential to provide semiquantitative information on annual rainfall variability in the past.

#### 4.5. Uranium: The Complex Story

The correlation between U and Sr-Ba- $\delta^{13}\text{C}$ , reflected in their overall synchronism and the coincidence of their minima (Fig. 6), suggests that calcite precipitation in the karst aquifer is also a relevant mechanism influencing the temporal variation of the U concentration in the river water. This is consistent with the calcite-water distribution coefficient for  $\text{UO}_2^{2+}$ , which is quite low and similar to that of Sr and Ba (Kitano and Oomori, 1971).

Nonetheless, obvious differences between the U pattern and the record of Sr, Ba, and  $\delta^{13}\text{C}$  exist. The U variation shows a markedly higher seasonal amplitude, a more pronounced annual cycle, and is characterized by conspicuous maxima, which are almost completely absent in the patterns of the other three variables. These differences imply that calcite precipitation is only one of several geochemical processes controlling U variability. In contrast to Sr and Ba, the mobility of U in natural waters is greatly influenced by changes of the redox state, adsorption onto various materials, and the availability of organic and inorganic complex ligands (e.g., Langmuir, 1978; Porcelli et al., 1997; Andersson et al., 1998). Redox changes are most probably unimportant as a control on U solubility because the water is likely to be well oxygenated throughout the year. Furthermore, the relatively high alkalinity of the water increases the stability of U in the form of dissolved carbonate complexes. Potentially, U may be removed from solution by adsorption onto Fe-oxyhydroxides, clays and other secondary minerals (e.g., Andersson et al., 1998), which could be enhanced during the wet season when the concentration of suspended particulate matter in the river is markedly higher than during the dry season. While this seasonally variable scavenging could theoretically explain relatively high U concentrations in the tufa during dry seasons, and relatively low concentrations during wet seasons, it is unlikely to account for the characteristic maxima of the U record. The latter suggest that the flux of U to the water table is probably increased during certain periods.

A peculiarity of the U pattern is the alternation of high and low dry season maxima. Comparison with the precipitation record (Fig. 6) shows that this alternation mimics the biennial variation in wet season rainfall. Relatively high dry season U concentrations in the tufa occur after wet seasons with high rainfall, and relatively low dry season concentrations follow wet seasons with low rainfall. The relationship between the two records is most striking during the period from 1986 to 1994 and blurs somewhat toward the end of the 1990s (Fig. 6). It is therefore likely that the transfer of U to the river water is linked to the amount of wet season rainfall.

We suggest that during intensive rain events relatively high amounts of humic and fulvic substances are mobilized from the soil zone. U which is strongly retained in the soil under normal recharge conditions (Mangini et al., 1979), is complexed by the organic colloids and carried to the water table. The importance of humate and fulvate complexes for the transport of U has been demonstrated in several studies (e.g., Dearlove et al., 1991; Read et al., 1993; Porcelli et al., 1997; Riotte and Chabaux, 1999). By contrast, during wet seasons with relatively low rainfall the mobilization of dissolved organic carbon from the soil is suppressed, resulting in lower U concentrations

in the river water. From the relationship between wet season rainfall and the U concentration in the tufa (Fig. 6) it is evident, that the waters enriched in organic colloids and U contribute to discharge within several months after the rain event. Therefore, these waters are derived from a storage system with a relatively short water residence time, most probably the larger joints and fissures of the karst aquifers.

To explain both the correlation of U with Sr-Ba- $\delta^{13}\text{C}$  and the increased U concentrations after “wet” rainy seasons, we suggest that U is contributed from two distinct sources. Groundwater stored in small-scale fissures and the porous matrix of the karst supplies U that is mainly derived from bedrock (i.e., limestone and dolomite) dissolution. The U content of this component is relatively low and is modulated by calcite precipitation in the karst. The latter gives rise to a positive correlation between Sr, Ba,  $\delta^{13}\text{C}$  and U in these waters. As described previously, the variations of Sr, Ba, and  $\delta^{13}\text{C}$  in the tufa are primarily controlled by the chemistry of this water component, which has a residence time of  $\sim 1$  to 2 yr in the karst. The U content, on the other hand, is further influenced by a second component which discharges within a few months after the rain event. Depending on the amount of rainfall during the wet season, these waters are variably enriched in U, resulting in more or less elevated dry season concentrations in the tufa record.

Since U derived from bedrock dissolution and U mobilized from the soil zone potentially have distinct ( $^{234}\text{U}/^{238}\text{U}$ ) activity ratios (Riotte and Chabaux, 1999), we will carry out a supplementary U isotope study to verify the proposed two-component mixing model.

## 5. CONCLUSIONS

Our study demonstrates the capability of fluvial tufas to preserve high-resolution climate information in the form of internally consistent seasonal trace element and stable isotope variations. A cornerstone of our approach was the development of a reliable time series for the sampled profile based on the temperature dependence of the  $\delta^{18}\text{O}$  signal. The accurate chronology allowed us to compare the data sets with available meteorological and hydrological observations. This opportunity, as well as the combined trace element and stable isotope approach, were essential to overcome the numerous problems generally hampering a straightforward interpretation of chemical records in freshwater carbonates. As a consequence, it was possible to constrain the relevant geochemical processes relating climate variables, such as temperature and precipitation, to their chemical proxies in the tufa record.

The most promising outcome of this study is probably the “rediscovery” of Mg as a potentially useful thermometer in terrestrial carbonates. We have shown that temperatures calculated from the Mg concentrations of the sample set provide close approximations of average annual water temperature variations. Furthermore, temporal changes in  $(\text{Mg}/\text{Ca})_{\text{water}}$  can be estimated using an empirically derived equation, relating  $(\text{Mg}/\text{Ca})_{\text{water}}$  to the  $(\text{Sr}/\text{Ba})$  ratio measured in the tufa samples. By means of this relationship it is theoretically possible to determine the  $(\text{Mg}/\text{Ca})$  ratio of paleowaters, and hence to derive reliable estimates of former water temperatures from the Mg concentrations of fossil tufas. With this independent temperature information, it is thus

feasible to quantify temporal variations in  $\delta^{18}\text{O}_{\text{water}}$ , which provides an additional source of valuable information on the hydrological cycle. While the correlation between  $(\text{Mg}/\text{Ca})_{\text{water}}$  and  $(\text{Sr}/\text{Ba})_{\text{tufa}}$ , described in this article, applies only to the catchment of the Gregory River, it is likely that similar relationships exist in other karst environments. Revealing these relationships will help to fully exploit the potential of both Mg thermometry and  $\delta^{18}\text{O}$  in terrestrial carbonates.

The sympathetic variations in Sr, Ba, and  $\delta^{13}\text{C}$  in the tufa record changes in water chemistry, which are mainly caused by variable amounts of calcite precipitation within the vadose zone of the karst aquifer. The latter is thought to be markedly subdued whenever the amount of wet season precipitation exceeds a certain threshold. Accordingly, pronounced minima in the patterns of Sr, Ba, and  $\delta^{13}\text{C}$  are interpreted to reflect years with above-average rainfall. Due to the water residence time in the karst, these proxy signals in the tufa record are delayed by 1 to 2 yr. Nonetheless, the amplitudes of the minima are proportional to the cumulative rainfall during the related wet seasons. Therefore, it appears possible to use Sr, Ba, and  $\delta^{13}\text{C}$  records of fossil tufas to obtain semiquantitative information on annual rainfall variability in the past.

The pronounced seasonal and annual variation in the U concentration of the tufa samples is thought to mainly reflect changes in the U flux from the soil zone to the water table. While U is strongly retained in the soil under normal recharge conditions, it is transported to the phreatic zone by complexing organic colloids during intensive rain events. Therefore, the U concentration in the tufa record shows conspicuous maxima several months after above-average wet seasons. In this context it is remarkable that the U pattern mimics the biennial rainfall cycle, which is the dominant form of monsoon variability throughout the Indopacific (e.g., Meehl, 1994). Combined with the information gained from Sr, Ba, and  $\delta^{13}\text{C}$ , U records from fossil tufas may therefore provide new insights into temporal changes in high-frequency monsoon variability.

The next step will be to scrutinize the effects of recrystallization and diagenetic alteration on the preservation of fossil tufa records. If tufa deposits turn out to be reasonably resistant to secondary processes, combined investigation of speleothems and tufas from the same area could become a promising approach in future research. While speleothems record long-term changes in paleoenvironmental conditions, tufas could provide information on annual and subannual climate variability during selected periods of the past.

*Acknowledgments*—I am grateful to Geoff Pocock from the Department of Natural Resources in Ayr for providing the river discharge and water temperature data, as well as for his enthusiasm in answering my questions. Further thanks go to Joe Cali (ANU) for his help with stable isotope measurements, and to Julian Andrews and three anonymous referees who provided suggestions for improvement of the manuscript. Receipt of a Ph.D. scholarship from La Trobe University is gratefully acknowledged. Last but not least, I thank my parents, Ingeborg and Hans-Georg Ihlenfeld, as well as my partner Tania Dee, for their invaluable support. This research project was funded by an ARC small grant to Roland Maas and John Webb.

*Associate editor:* R. H. Byrne

## REFERENCES

- Andersson P. S., Porcelli D., Wasserburg G. J., and Ingri J. (1998) Particle transport of  $^{234}\text{U}$ - $^{238}\text{U}$  in the Kalix River and in the Baltic Sea. *Geochim. Cosmochim. Acta* **62**, 385–392.
- Andrews J. E., Riding R., and Dennis P. F. (1993) Stable isotopic compositions of recent freshwater cyanobacterial carbonates from the British Isles: Local and regional environmental controls. *Sedimentology* **40**, 303–314.
- Andrews J. E., Pedley H. M., and Dennis P. F. (1994) Stable isotope record of palaeoclimate change in a British Holocene tufa. *Holocene* **4**, 349–355.
- Andrews J. E., Riding R., and Dennis P. F. (1997) The stable isotope record of environmental and climatic signals in modern terrestrial microbial carbonates from Europe. *Palaeogeogr. Palaeoclimatol. Palaeoecol.* **129**, 171–189.
- Andrews J. E., Pedley M., and Dennis P. F. (2000) Palaeoenvironmental records in Holocene Spanish tufas: A stable isotope approach in search of reliable climatic archives. *Sedimentology* **47**, 961–978.
- Ayalon A., Bar-Matthews M., and Sass E. (1998) Rainfall-recharge relationships within a karstic terrain in the eastern Mediterranean semi-arid region, Israel:  $\delta^{18}\text{O}$  and  $\delta\text{D}$  characteristics. *J. Hydrol.* **207**, 18–31.
- Ayalon A., Bar-Matthews M., and Kaufman A. (1999) Petrography, strontium, barium and uranium concentrations, and strontium and uranium isotope ratios in speleothems as paleoclimatic proxies: Soreq cave, Israel. *Holocene* **9**, 715–722.
- Baker A., Genty D., Dreybrodt W., Barnes W. L., Mockler N. J., and Grapes J. (1998) Testing theoretically predicted stalagmite growth rate with recent annually laminated samples: Implications for past stalagmite deposition. *Geochim. Cosmochim. Acta* **62**, 393–404.
- Bar-Matthews M., Ayalon A., Matthews A., Sass E., and Halicz L. (1996) Carbon and oxygen isotope study of the active water-carbonate system in a karstic Mediterranean cave: Implications for paleoclimate research in semiarid regions. *Geochim. Cosmochim. Acta* **60**, 337–347.
- Bar-Matthews M., Ayalon A., and Kaufman A. (1997) Late Quaternary paleoclimate in the eastern Mediterranean region from stable isotope analysis of speleothems at Soreq cave, Israel. *Quat. Res.* **47**, 155–168.
- Bar-Matthews M., Ayalon A., Kaufman A., and Wasserburg G. J. (1999) The eastern Mediterranean paleoclimate as a reflection of regional events: Soreq cave, Israel. *Earth Planet. Sci. Lett.* **166**, 85–95.
- Budd A. R., Hazell M., Sedgmen A., Sedgmen L., Wyborn L. A. I., and Ryburn R. J. (2000) *OZCHEM: National Whole Rock Geochemistry Database*, AGSO Record 2000/12. Australian Geological Survey Organisation.
- Burton E. A. and Walter L. M. (1991) The effects of  $\text{P}_{\text{CO}_2}$  and temperature on magnesium incorporation in calcite in seawater and  $\text{MgCl}_2$ - $\text{CaCl}_2$  solutions. *Geochim. Cosmochim. Acta* **55**, 777–785.
- Cerling T. E., Quade J., Solomon D. K., and Bowman J. R. (1991) On the carbon isotopic composition of soil carbon dioxide. *Geochim. Cosmochim. Acta* **55**, 3403–3405.
- Chafetz H. S., Utech N. M., and Fitzmaurice S. P. (1991) Differences in the  $\delta^{18}\text{O}$  and  $\delta^{13}\text{C}$  signatures of seasonal laminae comprising travertine stromatolites. *J. Sediment. Petrol.* **61**, 1015–1028.
- Charles C. D., Hunter D. E., and Fairbanks R. G. (1997) Interaction between the ENSO and the Asian monsoon in a coral record of tropical climate. *Science* **277**, 925–928.
- Dearlove J. L. P., Longworth G., Ivanovich M., Kim J.-I., Delakowitz B., and Zeh P. (1991) Study of groundwater colloids and their geochemical interactions with natural radionuclides in Gorleben aquifer systems. *Radiochim. Acta* **52/53**, 83–89.
- Dickson J. A. D. (1991) Disequilibrium carbon and oxygen isotope variations in natural calcite. *Nature* **353**, 842–844.
- Drysdale R. N., Taylor M. P. and Ihlenfeld C. (2002) Factors controlling the chemical evolution of travertine-depositing rivers of the Barkly Karst, northern Australia. *Hydrol. Proc.*, **16**, 2941–2962 (2002).
- Epstein S. and Mayeda T. K. (1953) Variations of the  $^{18}\text{O}/^{16}\text{O}$  ratio in natural waters. *Geochim. Cosmochim. Acta* **4**, 213–224.
- Even H., Carmi I., Magaritz M., and Gerson R. (1986) Timing the transport of waters through the upper vadose zone in a karstic system above a cave in Israel. *Earth Surf. Proc. Landform* **11**, 181–191.
- Fairchild I. J., Borsato A., Tooth A. F., Frisia S., Hawkesworth C. J., Huang Y.-M., McDermott F., and Spiro B. (2000) Controls on trace element (Sr-Mg) compositions of carbonate cave waters: Implications for speleothem climatic records. *Chem. Geol.* **166**, 255–269.
- Gascoyne M. (1983) Trace element partition coefficients in the calcite-water system and their palaeoclimatic significance in cave studies. *J. Hydrol.* **61**, 213–222.
- Goede A. (1994) Continuous early last glacial palaeoenvironmental record from a Tasmanian speleothem based on stable isotope and minor element variations. *Quat. Sci. Rev.* **13**, 283–291.
- Goede A., McCulloch M. T., McDermott F., and Hawkesworth C. J. (1998) Aeolian contribution to strontium and strontium isotope variations in a Tasmanian speleothem. *Chem. Geol.* **149**, 37–50.
- Gonfiantini R. (1986) Environmental isotopes in lake studies. In *Handbook of Environmental Isotope Geochemistry*, Vol. 2, *The Terrestrial Environment*, B (eds. P. Fritz and J.-Ch. Fontes), pp. 113–168. Elsevier.
- Hellstrom J. C. and McCulloch M. T. (2000) Multi-proxy constraints on the climatic significance of trace element records from a New Zealand speleothem. *Earth Planet. Sci. Lett.* **179**, 287–297.
- Hendy C. H. (1971) The isotopic geochemistry of speleothems—I. The calculation of the effects of different modes of formation on the isotopic composition of speleothems and their applicability as palaeoclimatic indicators. *Geochim. Cosmochim. Acta* **35**, 801–824.
- Howson M. R., Pethybridge A. D., and House W. A. (1987) Synthesis and distribution coefficient of low-magnesium calcites. *Chem. Geol.* **64**, 79–87.
- Huang Y.-M. and Fairchild I. J. (2001) Partitioning of  $\text{Sr}^{2+}$  and  $\text{Mg}^{2+}$  into calcite under karst-analogue experimental conditions. *Geochim. Cosmochim. Acta* **65**, 47–62.
- Huang Y.-M., Fairchild I. J., Borsato A., Frisia S., Cassidy N. J., McDermott F., and Hawkesworth C. J. (2001) Seasonal variations in Sr, Mg and P in modern speleothems (Grotta di Ernesto, Italy). *Chem. Geol.* **175**, 429–448.
- Johnson B. J., Miller G. H., Fogel M. L., Magee J. W., Gagan M. K., and Chivas A. R. (1999) 65,000 yr of vegetation change in central Australia and the Australian summer monsoon. *Science* **284**, 1150–1152.
- Kitano Y. and Oomori T. (1971) The coprecipitation of uranium with calcium carbonate. *J. Oceanogr. Soc. Jpn.* **27**, 34–42.
- Lakey B. and Krothe N. C. (1996) Stable isotopic variation of storm discharge from a perennial karst spring, Indiana. *Water Resour. Res.* **32**, 721–731.
- Langmuir D. (1978) Uranium solution-mineral equilibria at low temperatures with applications to sedimentary ore deposits. *Geochim. Cosmochim. Acta* **42**, 547–569.
- Langmuir D. and Herman J. S. (1980) The mobility of thorium in natural waters at low temperatures. *Geochim. Cosmochim. Acta* **44**, 1753–1766.
- Lorens R. B. (1981) Sr, Cd, Mn and Co distribution coefficients in calcite as a function of calcite precipitation rate. *Geochim. Cosmochim. Acta* **45**, 553–561.
- Mangini A., Sonntag C., Bertsch G., and Müller E. (1979) Evidence for a higher natural uranium content in world rivers. *Nature* **278**, 337–339.
- McBride M. B. (1994) *Environmental Chemistry of Soils*. Oxford University Press.
- McConnaughey T. A. (1989)  $^{13}\text{C}$  and  $^{18}\text{O}$  isotopic disequilibria in biological carbonates, I. Patterns. *Geochim. Cosmochim. Acta* **53**, 151–162.
- McCrea J. M. (1950) On the isotope chemistry of carbonates and a paleotemperature scale. *J. Chem. Phys.* **18**, 849–857.
- McDermott F., Frisia S., Huang Y.-M., Longinelli A., Spiro B., Heaton T. H. E., Hawkesworth C. J., Borsato A., Keppens E., Fairchild I. J., van der Borg K., Verheyden S., and Selmo E. (1999) Holocene climate variability in Europe: Evidence from  $\delta^{18}\text{O}$ , textural and extension-rate variations in three speleothems. *Quat. Sci. Rev.* **18**, 1021–1038.
- Meehl G. A. (1994) Coupled land-ocean-atmosphere processes and South Asian monsoon variability. *Science* **266**, 263–267.

- Merz-Preiss M. and Riding R. (1999) Cyanobacterial tufa calcification in two freshwater streams: Ambient environment, chemical thresholds and biological processes. *Sediment. Geol.* **126**, 103–124.
- Montoya M., Crowley T. J., and von Storch H. (1998) Temperatures at the last interglacial simulated by a coupled ocean-atmosphere climate model. *Paleoceanography* **13**, 170–177.
- Mook W. G., Bommerson J. C., and Staverman W. H. (1974) Carbon isotope fractionation between dissolved bicarbonate and gaseous carbon dioxide. *Earth Planet. Sci. Lett.* **22**, 169–176.
- Mucci A. (1987) Influence of temperature on the composition of magnesian calcite overgrowths precipitation from seawater. *Geochim. Cosmochim. Acta* **51**, 1977–1984.
- Mucci A. and Morse J. W. (1983) The incorporation of  $Mg^{2+}$  and  $Sr^{2+}$  into calcite overgrowths: Influences of growth rate and solution composition. *Geochim. Cosmochim. Acta* **47**, 217–233.
- Nesbitt H. W., Markovics G., and Price R. C. (1980) Chemical processes affecting alkalis and alkaline earths during continental weathering. *Geochim. Cosmochim. Acta* **44**, 1659–1666.
- O'Neil J. R., Clayton R. N., and Mayeda T. K. (1969) Oxygen isotope fractionation in divalent metal carbonates. *J. Chem. Phys.* **51**, 5547–5558.
- Oomori T., Kaneshima H., Maezato Y., and Kitano Y. (1987) Distribution coefficient of  $Mg^{2+}$  ions between calcite and solution at 10–50°C. *Mar. Chem.* **20**, 327–336.
- Paquette J. and Reeder R. J. (1995) Relationship between surface structure, growth mechanism and trace element incorporation in calcite. *Geochim. Cosmochim. Acta* **59**, 735–749.
- Pazdur A., Pazdur M. F., Starkel L., and Szulc J. (1988) Stable isotopes of Holocene calcareous tufa in southern Poland as paleoclimatic indicators. *Quat. Res.* **30**, 177–189.
- Pentecost A. and Riding R. (1986) Calcification in cyanobacteria. In *Biomining in Lower Plants and Animals* (eds. B. S. C. Leadbeater and R. Riding), pp. 73–90. Special Publication 30. The Systematics Association, Clarendon Press, Oxford.
- Pingitore N. E. and Eastman M. P. (1986) The coprecipitation of  $Sr^{2+}$  with calcite at 25°C and 1 atm. *Geochim. Cosmochim. Acta* **50**, 2195–2203.
- Porcelli D., Andersson P. S., Wasserburg G. J., Ingri J., and Baskaran M. (1997) The importance of colloids and mires for the transport of uranium isotopes through the Kalix river watershed and Baltic Sea. *Geochim. Cosmochim. Acta* **61**, 4095–4113.
- Rank D., Völkl G., Malozewski P., Stichter W. (1992) Flow dynamics in an alpine karst massif studied by means of environmental isotopes. In *Isotope Techniques in Water Resource Development 1991*, pp. 327–343. IAEA Symposium 319. March 1991, Vienna.
- Read D., Bennett D. G., Hooker P. J., Ivanovich M., Longworth G., Milodowski A. E., and Noy D. J. (1993) The migration of uranium into peat-rich soils at Broubster, Caithness, Scotland, UK. *J. Contaminant Hydrol.* **13**, 291–308.
- Reeve A. S. and Perry E. C. (1994) Carbonate geochemistry and the concentrations of aqueous  $Mg^{2+}$ ,  $Sr^{2+}$  and  $Ca^{2+}$ : Western north coast of the Yucatan, Mexico. *Chem. Geol.* **112**, 105–117.
- Riotte J. and Chabaux F. (1999) ( $^{234}U/^{238}U$ ) activity ratios in freshwaters as tracers of hydrological processes: The Strengbach watershed (Vosges, France). *Geochim. Cosmochim. Acta* **63**, 1263–1275.
- Roberts M. S., Smart P. L., and Baker A. (1998) Annual trace element variations in a Holocene speleothem. *Earth Planet. Sci. Lett.* **154**, 237–246.
- Roberts M. S., Smart P. L., Hawkesworth C. J., Perkins W. T., and Pearce N. J. G. (1999) Trace element variations in coeval Holocene speleothems from GB cave, southwest England. *Holocene* **9**, 707–713.
- Rollins L. (1987) PCWATEQ. Computer program. Woodland, Calif.: Shadoware.
- Romanek C. S., Grossman E. L., and Morse J. W. (1992) Carbon isotopic fractionation in synthetic aragonite and calcite: Effects of temperature and precipitation rate. *Geochim. Cosmochim. Acta* **56**, 419–430.
- Rozanski K., Araguás-Araguás L., and Gonfiantini R. (1993) Isotopic patterns in modern global precipitation. In *Climate Change in Continental Isotopic Records* (ed. P. K. Swart et al), pp. 1–36. Monograph 78. AGU.
- Tesoriero A. J. and Pankow J. F. (1996) Solid solution partitioning of  $Sr^{2+}$ ,  $Ba^{2+}$  and  $Cd^{2+}$  into calcite. *Geochim. Cosmochim. Acta* **60**, 1053–1063.
- Tudhope A. W., Chilcott C. P., McCulloch M. T., Cook E. R., Chappell J., Ellam R. M., Lea D. W., Lough J. M., and Shimmield G. B. (2001) Variability in the El Niño-Southern Oscillation through a glacial-interglacial cycle. *Science* **291**, 1511–1517.
- Veizer J., Ala D., Azmy K., Bruckschen P., Buhl D., Bruhn F., Carden G. A. F., Diener A., Ebner S., Godderis Y., Jasper T., Korte C., Pawellek F., Podlaha O. G., and Strauss H. (1999)  $^{87}Sr/^{86}Sr$ ,  $\delta^{13}C$  and  $\delta^{18}O$  evolution of Phanerozoic seawater. *Chem. Geol.* **161**, 59–88.
- Vogel J. C. (1993) Variability of carbon isotope fractionation during photosynthesis. In *Stable Isotopes and Plant Carbon-Water Relations* (ed. J. R. Ehleringer et al), pp. 29–38. Academic Press.
- Zhong S. and Mucci A. (1989) Calcite and aragonite precipitation from seawater solutions of various salinities: Precipitation rates and overgrowth compositions. *Chem. Geol.* **78**, 283–299.

## APPENDIX

Table A1. Element concentrations and stable isotope compositions (‰) for the sampled tufa profile.

Sample	Time <sup>a</sup> (yr AD)	Mg (ppm)	Sr (ppm)	Ba (ppm)	U (ppm)	Th (ppb)	$\delta^{13}C$ (PDB)	$\delta^{18}O$ (SMOW)
GMT-1	1999.39	8480	168.1	185.6	1.149	27.6	-8.56	20.81
GMT-2	1999.00	8747	155.1	185.5	0.745	67.3	-8.57	20.10
GMT-3	1998.85	9301	155.8	171.2	0.714	34.9	-8.40	20.25
GMT-4	1998.73	8753	160.4	164.6	0.913	24.1	-8.52	20.55
GMT-5	1998.69	9545	157.7	155.5	0.912	13.9	-8.51	20.66
GMT-6	1998.53	8044	153.2	155.6	0.911	6.0	-8.58	20.88
GMT-7	1998.20	8485	144.8	152.9	0.858	89.7	-8.72	20.17
GMT-8	1998.06	9835	147.1	148.2	0.785	28.1	-8.61	20.05
GMT-9	1997.78	9463	162.7	156.3	1.218	14.0	-8.27	20.87
GMT-10	1997.55	8615	148.2	147.1	1.343	2.7	-8.30	21.09
GMT-11	1997.29	8319	158.8	162.1	1.392	37.9	-8.45	20.80
GMT-12	1997.00	9290	154.6	162.2	0.975	7.5	-8.47	20.42
GMT-13	1996.83	9366	142.4	142.1	0.787	26.9	-8.71	20.56

Continued

Table A1. Continued.

Sample	Time <sup>a</sup> (yr AD)	Mg (ppm)	Sr (ppm)	Ba (ppm)	U (ppm)	Th (ppb)	$\delta^{13}\text{C}$ (PDB)	$\delta^{18}\text{O}$ (SMOW)
GMT-14	1996.73	7431	154.3	160.5	1.075	2.2	-8.68	20.72
GMT-15	1996.60	8554	145.3	139.6	1.051	2.8	-8.66	20.87
GMT-16	1996.40	9139	150.2	146.5	0.980	24.3	-8.58	20.61
GMT-17	1996.28	10569	157.9	158.7	0.983	76.3	-8.46	20.33
GMT-18	1996.00	10362	146.7	149.3	0.761	19.3	-8.42	19.77
GMT-19	1995.83	10642	157.9	143.6	1.035	0.3	-8.39	20.12
GMT-20	1995.55	9327	173.2	179.7	1.349	4.2	-8.21	20.80
GMT-21	1995.40	9413	169.0	151.4	1.406	5.3	-8.43	20.63
GMT-22	1995.23	11027	157.7	152.9	0.896	26.6	-8.60	20.11
GMT-23	1995.07	11834	148.0	143.2	0.626	2.6	-8.45	20.28
GMT-24	1994.94	10429	118.6	114.9	0.563	14.9	-8.99	20.37
GMT-25	1994.78	10659	97.9	95.7	0.594	57.4	-9.21	20.35
GMT-26	1994.68	9022	126.6	125.5	0.956	7.8	-8.90	20.80
GMT-27	1994.57	8813	155.8	145.3	1.360	14.1	-8.54	21.07
GMT-28	1994.43	9024	147.2	142.5	1.039	11.3	-8.43	21.01
GMT-29	1994.36	9683	166.1	157.6	1.221	3.6	-8.29	20.87
GMT-30	1994.20	10295	151.7	157.4	0.853	7.4	-8.42	20.46
GMT-31	1994.07	10544	136.0	137.1	0.737	37.1	-8.44	20.16
GMT-32	1994.00	10788	137.9	138.4	0.952	21.3	-8.47	20.08
GMT-33	1993.86	10290	139.7	136.5	1.261	12.4	-8.46	20.31
GMT-34	1993.50	7791	177.2	180.1	2.465	8.1	-8.46	20.66
GMT-35	1992.92	9702	142.3	147.7	1.105	37.1	-8.58	20.19
GMT-36	1992.55	7851	143.7	145.5	1.168	1.6	-9.03	20.41
GMT-37	1992.32	7980	146.3	160.0	1.233	82.9	-8.83	20.08
GMT-38	1992.05	10606	151.2	151.9	0.827	3.2	-8.24	19.64
GMT-39	1991.84	9571	166.4	170.9	0.766	4.4	-8.20	20.03
GMT-40	1991.73	9045	165.5	171.7	0.882	18.7	-8.42	20.26
GMT-41	1991.50	8699	164.3	168.9	0.946	8.5	-8.39	20.58
GMT-42	1991.15	8832	170.3	178.6	1.729	37.0	-8.34	20.09
GMT-43	1990.96	9953	139.5	141.6	1.106	57.9	-8.26	20.41
GMT-44	1990.80	10280	152.0	140.3	1.133	3.0	-8.46	20.36
GMT-45	1990.56	8107	157.4	153.4	1.476	21.7	-8.42	21.02
GMT-46	1990.40	9975	155.7	145.7	1.198	14.1	-8.26	20.70
GMT-47	1990.31	10633	139.5	136.7	0.873	31.5	-8.39	20.44
GMT-48	1990.21	10249	112.2	112.7	0.723	69.5	-8.85	20.13
GMT-49	1990.08	10402	131.6	127.7	0.931	64.2	-8.96	20.09
GMT-50	1989.89	9585	138.2	131.1	1.036	11.9	-8.67	20.05
GMT-51	1989.80	9385	152.7	145.1	1.231	1.6	-8.50	20.33
GMT-52	1989.68	8020	150.2	143.8	1.349	18.5	-8.60	20.89
GMT-53	1989.57	7654	168.3	163.8	1.591	2.4	-8.31	21.20
GMT-54	1989.36	9025	157.3	152.8	1.062	28.3	-8.41	20.33
GMT-55	1989.26	8843	136.0	138.1	0.870	62.1	-8.67	20.57
GMT-56	1989.16	9285	123.2	122.6	0.734	86.1	-9.02	20.18
GMT-57	1988.98	10059	136.9	129.9	0.841	8.5	-8.78	19.66
GMT-58	1988.85	9663	161.1	147.0	1.029	12.4	-8.50	19.96
GMT-59	1988.58	8408	164.8	154.1	1.132	2.8	-8.41	20.64
GMT-60	1988.28	9002	174.2	159.0	1.206	16.2	-8.40	20.43
GMT-61	1988.13	9391	150.3	147.7	0.993	53.6	-8.39	20.21
GMT-62	1987.98	10192	167.3	150.2	1.065	12.9	-8.27	20.09
GMT-63	1987.88	9662	159.9	145.3	1.143	9.2	-8.38	20.22
GMT-64	1987.69	9247	168.8	151.0	1.520	3.2	-8.20	20.69
GMT-65	1987.60	8964	164.8	143.2	1.853	19.8	-8.19	20.84
GMT-66	1987.44	8864	165.3	148.4	1.768	18.6	-8.24	20.80
GMT-67	1987.25	9534	156.7	147.4	1.355	41.5	-8.21	20.44
GMT-68	1987.15	8669	148.4	145.5	1.078	81.0	-8.49	21.49
GMT-69	1986.93	9440	136.4	127.8	0.915	51.6	-8.61	20.51
GMT-70	1986.78	9094	139.4	134.3	1.065	6.3	-8.51	20.52
GMT-71	1986.58	9810	150.8	137.5	1.233	28.9	-8.31	20.78
GMT-72	1986.50	9922	146.7	141.5	1.208	38.5	-8.27	20.69
GMT-73	1986.15	10486	148.3	137.3	1.293	60.1	-8.39	20.03
GMT-74	1985.99	12053	155.1	133.4	1.292	48.9	-8.14	20.00
GMT-75	1985.90	12175	148.3	134.1	1.156	41.0	-8.14	20.20
GMT-76	1985.87	11193	130.5	122.0	0.991	32.1	-8.38	20.34
GMT-77	1985.83	9814	136.8	129.0	1.474	17.0	-8.61	20.52
GMT-78	1985.75	8637	155.6	147.0	2.147	10.0	-8.39	20.86

Continued

Table A1. Continued.

Sample	Time <sup>a</sup> (yr AD)	Mg (ppm)	Sr (ppm)	Ba (ppm)	U (ppm)	Th (ppb)	$\delta^{13}\text{C}$ (PDB)	$\delta^{18}\text{O}$ (SMOW)
GMT-79	1985.73	9033	154.0	134.1	1.607	1.1	-8.45	20.90
GMT-80	1985.69	9487	157.2	129.7	1.585	1.7	-8.38	21.01
GMT-81	1985.57	8936	160.6	147.6	1.712	10.6	-8.05	21.32
GMT-82	1985.32	9584	155.1	137.3	1.283	29.2	-8.30	20.64
GMT-83	1985.23	10071	157.6	144.1	1.144	32.9	-8.40	20.27
Mean		9480	151.1	147.0	1.132	25.2	-8.48	20.48
1 $\sigma$		971	14.0	16	0.336	23.3	0.22	0.38
RSD [%]		10.2	9.2	16.9	29.7	92.5	—	—

<sup>a</sup> Mean time of sample deposition (see section 4.1.2 for discussion).